Main Manuscript for

Distribution of phosphorylated alpha-synuclein in non-diseased brain implicates olfactory bulb mitral cells in synucleinopathy pathogenesis

Bryan A. Killinger[a], Gabriela Mercado[b], Solji Choi[a], Tyler Tittle[a], Yaping Chu[C], Patrik Brundin[b,d], and Jeffrey H. Kordower[C]

[a]Graduate College, Rush University Medical Center, Chicago Illinois 60612

[b] Parkinson's disease Center, Department of Neurodegenerative Science, Van Andel Institute, Grand Rapids MI 49503

[c] ASU-Banner Neurodegenerative Disease Research Center (NDRC), Arizona State University, Tempe Arizona 85287

[d]Pharma Research and Early Development (pRED), F Hoffman-La Roche, New York, USA

*Bryan A. Killinger

Email: bryan_killinger@rush.edu

Author Contributions: B.A.K. conceptualized studies, conducted studies, analyzed data, and wrote the manuscript. G.M. conducted some animal studies. S.C. and T.T. performed experiments and analyzed data. Y.C. was involved in human tissues processing. P.B. wrote manuscript and provided asyn knockout mice. J.H.K. wrote the manuscript.

Competing Interest Statement: P.B. is an employee of F Hoffman-La Roche and has consulted for Axial Therapeutics, Calico, CuraSen, Enterin Inc, Fujifilm-Cellular Dynamics Inc, Idorsia and Lundbeck A/S. He has received commercial support for research from Lundbeck A/S and Roche, and has ownership interests in Acousort AB, Axial Therapeutics, Enterin Inc and RYNE Biotechnology Inc. P.B. declares no non-financial interest. All other authors do not have any financial and non-financial interest to declare.

Keywords: Proteomics; neurodegeneration; vesicles; protein aggregation.

This PDF file includes:

Main Text
Figures 1 to 8
Table 1

Abstract

Synucleinopathies are neurodegenerative diseases characterized by pathological inclusions called “Lewy pathology” (LP) that consist of aggregated alpha-synuclein predominantly phosphorylated at serine 129 (PSER129). Despite the importance for understanding disease, little is known about the endogenous function of PSER129 or why it accumulates in disease. Here we conducted several observational studies using a sensitive tyramide signal amplification (TSA) technique to determine PSER129 distribution and function in the non-diseased mammalian brain. In wild-type non-diseased mice, PSER129 was detected in the olfactory bulb (OB) and several brain regions across the neuroaxis (i.e., OB to brain stem). In contrast, PSER129 immunoreactivity was not observed in any brain region of alpha-synuclein knockout mice. We found evidence of PSER129 positive structures in OB mitral cells of non-diseased mice, rats, non-human primates, and healthy humans. Using TSA multiplex fluorescent labeling we show that PSER129 positive punctate structures occur within inactive (i.e., cfos negative) T-box transcription factor 21 (TBX21) positive mitral cells and PSER129 within these cells was spatially associated with PK-resistant alpha-synuclein. Ubiquitin was found in PSER129 mitral cells but was not closely associated with PSER129. Biotinylation by antigen recognition (BAR) identified 125 PSER129-interacting proteins in the OB of healthy mice, which were significantly enriched for presynaptic vesicle trafficking/recycling, SNARE, fatty acid oxidation, oxidative phosphorylation, and RNA binding. TSA multiplex labeling confirmed the physical association of BAR identified protein Ywhag with PSER129 in the OB and in other regions across the neuroaxis. We conclude that PSER129 accumulates in mitral cells of the healthy OB as part of alpha-synuclein normal cellular functions. Incidental LP has been reported in the OB, and therefore we speculate that for synucleinopathies either; the disease processes begin locally in OB mitral cells or a systemic disease process is most apparent in the OB because the natural tendency to accumulate PSER129.

Significance Statement

Multiple lines of evidence have suggested that the disease process in some synucleinopathies begins in the olfactory bulb. Here we demonstrated that disease-associated phosphorylated alpha-synuclein preferentially occurs in mitral cells of the healthy mammalian olfactory bulb. We identified the protein interactome of phosphorylated alpha-synuclein in the healthy mouse olfactory bulb and established phosphorylated alpha-synuclein associates with presynaptic glutamatergic vesicles, SNARE machinery, and RNA metabolism machinery. Our data implicates olfactory bulb mitral cells in synucleinopathy pathogenesis. These findings advance our understanding of synucleinopathy disease origins and set the stage for new experimental models to interrogate the pathogenesis of synucleinopathies.

Main Text

Introduction

Synucleinopathies such as Parkinson's disease (PD), Multiple systems atrophy (MSA), and Dementia with Lewy bodies (DLB) are a group of neurodegenerative diseases characterized by intracellular alpha-synuclein aggregates called "Lewy pathology" (LP). In synucleinopathies, the distribution of LP has been suggested to adopt one of several characteristic patterns, engaging specific brain regions, which has led to the development of pathology staging schemes (1, 2). The brain structure that LP is most consistently found in is the olfactory bulb (OB), where LP is often detected in both the diseased and occasionally in the non-diseased brain (i.e., incidental LP) (2-4). It remains unclear why the OB commonly exhibits LP in the human brain, but one possibility is this structure may be prone to misfolding and accumulation of alpha-synuclein, especially during normal aging (5). Hyposmia is a common prodromal symptom of PD/DLB (6-9) supporting the hypothesis that the neurodegenerative process begins in the OB (10, 11) years prior to the onset of motor symptoms in PD or cognitive decline in DLB.

LP are complex molecularly heterogeneous intracellular structures containing proteinase K (PK) resistant filaments made of misfolded alpha-synuclein predominantly phosphorylated at serine 129 (PSER129). LP also contain numerous other proteins (i.e., ubiquitin, p62 etc.) along with fragmented organelles and lipids (12, 13) and a diverse array of alpha-synuclein proteoforms (14). Although alpha-synuclein is predominantly phosphorylated in LP, it has been estimated that less than 4% of the total endogenous alpha-synuclein pool is phosphorylated (15). The enrichment of PSER129 in LP strongly suggests this post-translation modification (PTM) plays a role in the disease process, but the exact role of PSER129, pathogenic or endogenous, remains unclear. Investigations have primarily focused on whether PSER129 promotes or inhibits alpha-synuclein accumulation as targeting the responsible kinases and/or phosphatases may be a viable therapeutic strategy. To date, PSER129 remains an agnostic proxy for the synucleinopathy disease process. The development of sensitive and specific antibodies to PSER129 has facilitated the detection of LP. However, the extent to which PSER129 can be present outside pathological LP aggregates is not clear, and it has been difficult to consistently detect low levels of endogenous PSER129 (16). For example previous attempts to identify endogenous PSER129 by immunohistochemistry (IHC) have been impeded by high affinity off-target binding of commercially available antibodies that interferes with on-target detection (16). Determining the role of endogenous PSER129 will help understand the disease process underlying synucleinopathies.

Here we present results of several observational studies investigating PSER129 in the brain and OB of healthy mammals.

Results

PSER129 Immunoreactivity in the Mouse Brain

PSER129 immunoreactivity was regionally specific across the WT mouse brain (Fig. 1A). PSER129 immunoreactivity was most apparent in the OB but also several other regions showed pronounced PSER129 immunoreactivity including the accessory OB (AOB), amygdala, nucleus accumbens, dentate gyrus, globus pallidus, hypothalamus, and substantia nigra reticulata (Fig. 1B). The brain stem and cerebellum lacked any discernable immunoreactivity with the notable exception of a group of weakly PSER129 positive cells in the dorsal motor nucleus of the vagus (*SI Appendix*, Fig. S1). Apparent nuclear immunoreactivity was observed in many cortical regions and the amygdala. Intense fiber staining was observed in the nucleus accumbens, dentate gyrus, entorhinal cortex, global pallidus, and substantia nigra pars compacta (Fig. 1B,C). PK digestion prior to IHC abolished PSER129 staining across the neuroaxis (Fig. 1B, “PK”). Immunoreactivity was weak when the primary antibody was pre-absorbed against the synthetic PSER129 peptide (Fig. 1B, “PA”), which is consistent with competitive binding of pre-absorbed monoclonal antibodies (*SI Appendix,* Fig. S2,F,G)(17). Staining was totally absent when the primary antibody was omitted from the staining protocol (Fig. 1B “-Primary”). PSER129 appeared variable between mice with some brains showing more prominent staining than others. In total, we observed positive PSER129 immunoreactivity in the OB of 13 out of 14 WT mice tested. In contrast, we did not observe PSER129 in 7 alpha-synuclein knockout mice tested in any brain region under any IHC conditions (Fig. 1B, “KO”). In the olfactory bulb of WT mice, processes and punctate structures were intensely labeled in the mitral cell layer, while in the external plexiform layer (EPL) and glomeruli (GM) were only weakly labeled (See Fig. 1D for annotated reference). Intense labeling of apparent cells and processes were observed in the AOB. PSER129 labeling was nearly absent in the granular layer (GL) and the olfactory nerve layer (ONL). Occasionally fibers projecting from mitral cells were observed in the inner plexiform layer (IPL).

To further investigate the specificity of PSER129 antibody EP1536Y we performed western blot (WB) on lysates from the mouse OB (Fig. 1E). Results showed a single 15-kDa band in the OB of WT mice that was absent from alpha-synuclein KO mice (Figure 1E, red arrow). A positive control sample (i.e., lysate from MSA striatum, Figure 1E “MSA”, *SI Appendix* Fig. S3) showed a major band at 15-kDa, as well as multiple high molecular weight species. Pretreatment of a duplicate blot with calf intestine alkaline phosphatase (Figure 1E, “Phosphatase”) abolished EP1536Y reactivity. We then probed for total alpha-synuclein using the “SYN1” antibody (Figure 1F) and observed a major band at 15-kDa in MSA and OB of WT mice as well as other high molecular weight species. Reactivity was not observed in alpha-synuclein KO mice and “SYN1” reactivity was similar with or without CIAP pretreatment.

148 **PSER129 Occurs as Punctate Structures in Mitral Cells**

149 We wanted to determine the intracellular distribution of PSER129 in the olfactory bulb
150 mitral cell layer. To do this we fluorescently labeled PSER129 in the OB of WT and M83 mice.
151 Results confirmed PSER129 signal in the mitral cell layer and diffuse punctate labeling in the
152 outer plexiform layer of WT mice. Punctate labeling was observed throughout the plexiform layer.
153 Cells within the mitral cell layer showed PSER129 granular staining in the nucleus and
154 perinuclear compartments. (Fig. 2A and B, green arrows). PSER129 and DAPI weakly
155 colocalized in these cells. M83 mice showed more prominent PSER129 labeling of the mitral cell
156 layer and strong fibers labeling in the plexiform layer (Fig. 2B). Within the mitral layer cells
157 showed strong nuclear and perinuclear PSER129 labeling. Punctate PSER129 labeling in the
158 outer plexiform layer extended to the glomerulus. PSER129 punctate staining was sporadically
159 observed in the granular layer of WT mice.

160 To determine if the punctate PSER129 staining originated in mitral cells we fluorescently
161 labeled both PSER129 and the mitral cell marker T-box transcription factor 21 (TBX21) using the
162 TSA multiplex protocol. This experiment was performed in the OB from healthy non-human
163 primates because the anti-TBX21 antibody used is of mouse origin, and therefore performing this
164 experiment on mouse tissues potentially would produce ambiguous results. We had already
165 observed the same PSER129 staining pattern in the non-human primate OB (see Fig. 3A and *SI*
166 *Appendix* Fig. S4) and therefore chose to assess PSER129 co-localization in this tissue. Results
167 show TBX21 labeling was predominantly nuclear, in select cells of the mitral layer (Fig. 2C,D).
168 TBX21 labeling was observed in some perinuclear structures. Perinuclear PSER129 puncta were
169 observed in TBX21 positive mitral cells. Within mitral cells PSER129 and TBX21 did not
170 colocalize (Fig. 2D).

171

172 **Mitral Cell PSER129 is Conserved Across Mammalian Species**

173 Next, we wanted to determine if PSER129 positive mitral cells were conserved across
174 species. To do this we stained for PSER129 in the OB of healthy rats, non-human primates (2
175 years of age), healthy adults, and individuals diagnosed with PD (see Table 1 for summary, for
176 detailed human data see *SI Appendix* Table S1). Result showed mitral cell staining in rats, non-
177 human primates, and humans, like what was observed in mice (Fig. 3A). Antibody clone psyn#64
178 also detected PSER129 in mitral cells like what we observed with antibody EP1536Y (*SI*
179 *Appendix* Fig. S4). In the OB of human PD, we found that HIAR (Heat induced antigen retrieval)
180 or PK digestion enhanced PSER129 detection, and in the healthy OB HIAR often enhanced
181 PSER129 staining (*SI Appendix* Fig. S5). PSER129 staining of the PD OB produces mostly
182 processes baring pathology, with a few cell bodies being immunoreactive. PSER129 positive
183 inclusions could be detected across all layers of the OB including the mitral cell layer, and most

184 prominently in the anterior olfactory nucleus (Fig. 3B,C). We attempted to verify that OB mitral
185 cells were intact in all samples by staining with the TBX21 antibody (*SI Appendix* Fig. S6),
186 however, we found immunoreactivity was absent from several human samples (Table 1) which
187 has been reported previously and may result from differences in post-mortem interval (18).

188 **PSER129 associates with PK-resistant alpha-synuclein in mouse mitral cells**

189 In human synucleinopathies and in synucleinopathy models aggregated alpha-synuclein
190 is predominantly phosphorylated (19). Previously we observed that PSER129 in the mouse OB
191 was PK-sensitive (Fig 1B, "PK") suggesting that this alpha-synuclein pool was not aggregated.
192 However, we previously observed unusual differential labeling in OB mitral cells, where "SYN1"
193 antibody reactivity in mitral cells appeared to inversely proportional to PSER129
194 immunoreactivity, suggesting that "SYN1" alpha-synuclein epitope (a.a. 91-98) was inaccessible
195 in PSER129 positive accumulations (*SI Appendix* Fig. S6). This suggested that alpha-synuclein
196 associated with PSER129 or PSER129 itself might be in complex or aggregated. To
197 experimentally test this possibility, we developed and used a new TSA multiplexing approach to
198 label PK resistant alpha-synuclein and PSER129 in the same tissue, while avoiding the
199 destroying the PSER129 epitope (Fig. 4A). This technique allowed us to assess the distribution of
200 PK-sensitive PSER129 in relation to PK-resistant alpha-synuclein.

201 We validated this approach by applying it to PD substantia nigra tissues (Fig 4B). Without
202 PK digestion alpha-synuclein signal is abundant and overlaps with PSER129 primarily in Lewy
203 bodies and Lewy neurites (Figure 4B, top panels). Samples processed with PK digestion show
204 markedly reduced alpha-synuclein signal with the remaining alpha-synuclein overlapping with
205 PSER129. Interestingly, complete overlap between alpha-synuclein and PSER129 was not
206 observed, even after PK digestion, suggesting these two antibodies preferentially label different
207 alpha-synuclein pools, a phenomenon that has been described in several other reports (20, 21)
208 and observed here (*SI appendix* Fig. S7).

209 We then applied this technique to mouse OB to determine if PSER129 was associated
210 with PK-resistant alpha-synuclein. Results show high alpha-synuclein content throughout the
211 layers of the OB (Figure 4C,D, top panels) when PK was omitted from the protocol. Alpha-
212 synuclein immunoreactivity was decreased in the OB following PK digestion with regional
213 immunoreactivity being preserved particularly in mitral cell layer, accessory OB, and apparent
214 fibers of the OB tract (Fig. 4C, D, bottom panels "PK"). High overlap between PSER129 and PK-
215 resistant alpha-synuclein was observed particularly in the mitral cell layer and accessory OB, but
216 to a lesser extent in the fibers of the OB tract, which were poorly labeled with PSER129 but
217 clearly labeled with PK-resistant alpha-synuclein. High magnification images of the mitral cells
218 and mitral cell projections (Fig. 4E and F) show selective overlap between the two signals.
219 Without PK, PSER129 overlaps well with total alpha-synuclein in projections of the outer

220 plexiform layer (Fig. 4F, top panel) but in the mitral cell body overlap was minimal with cytosolic
221 PSER129 puncta and nuclear PSER129 being spatially segregated from total alpha-synuclein
222 (Fig. 4E, top panel, white arrows). Remarkably, with PK digestion total alpha-synuclein and
223 PSER129 then showed high overlap in mitral cells, particularly in the nucleus and projections
224 (Figure 4E, F, Bottom panels, "PK"). Cytosolic PSER129 puncta were associated with faint PK-
225 resistant alpha-synuclein immunoreactivity (Fig 4E,"PK", white arrows and Fig 4G). Projection
226 images of single mitral cells showed small perinuclear PSER129 puncta and PSER129
227 surrounding mitral cells that were not associated with PK-resistant alpha-synuclein. Within the
228 dendrite and nucleus PSER129 and PK-resistant alpha-synuclein were closely, but not
229 completely, associated.
230
231 **PSER129 in mitral cells was not associated with ubiquitin**
232 Intraneuronal ubiquitin can accumulate with age and disease (22) and is enriched in LP,
233 particularly mature Lewy bodies (23). To determine if PSER129 positive mitral cells also
234 accumulated ubiquitin, we multiplex labeled ubiquitin and PSER129 in the mouse OB. Results
235 show that ubiquitin staining was observed throughout the layers of the OB (Fig. 5A). Cells near or
236 within the mitral layer were labeled for ubiquitin (Fig. 5B). Overlap between PSER129 and
237 ubiquitin was observed with confocal images taken at lower magnifications (Fig. 5C, D). However,
238 high-magnification confocal images showed little overlap between PSER129 and ubiquitin in
239 mitral cells (Fig. 5E). Ubiquitin could be found in both the cytosol and nucleus of PSER129 mitral
240 cells. Using the same multiplexing protocol, we found that, as expected, ubiquitin and PSER129
241 intensely labeled mature Lewy bodies in the PD substantia nigra (Fig. 5F). PSER129 also labeled
242 structures peripheral to Lewy bodies (Fig. 5F). Together these results demonstrated that unlike
243 mature LP, in mitral cells PSER129 was not strongly associated with ubiquitin accumulation.
244
245 **PSER129 Interacts Vesicle Cycle Machinery in the OB**
246 We had observed PSER129 staining in healthy OB, and this observation provided the
247 unique opportunity to study endogenous PSER129. To determine the functional relevance of the
248 apparent endogenous PSER129 pool, we measured the PSER129 interactome in the OB using a
249 proximity labeling technique we previously used to identify pathological alpha-synuclein
250 interactions in fixed tissues called BAR-PSER129 (24). We applied BAR-PSER129 to both WT
251 and alpha-synuclein KO mice. Dot blot following BAR-PSER129 shows enrichment for
252 biotinylated proteins and alpha-synuclein (Fig. 6A) only in WT mice. BAR-PSER129 conducted in
253 the absence of primary antibody ("Neg" or "-") showed minimal signal in WT and KO mice.
254 Next, we preformed liquid chromatography tandem mass spectrometry (LC-MS/MS) of
255 the BAR-PSER129 samples and identified a total of 241 proteins (*SI Appendix* Dataset S1), with

256 125 proteins (51.7% of those identified) being unique to BAR-PSER129 in WT OB (Fig. 6B and *SI*
257 *Appendix* Dataset S3). In agreement with dot blot results (Fig. 4A), alpha-synuclein was
258 exclusively identified in the BAR-PSER129 WT OB condition, with three exclusive unique spectra
259 comprising a 30% coverage of alpha-synuclein protein being detected in this sample (Figure 6C
260 and *SI Appendix* Dataset S2). Unbiased hierarchal clustering of identified proteins across
261 samples verified BAR-PSER129 WT OB sample segregated from all other capture conditions (*SI*
262 *appendix* Fig. S8). Amongst the BAR-PSER129 WT OB unique proteins were 5 kinases
263 (Camk2b, Pacsin1, Pdxk, Mapk1, and Dclk1) and 3 phosphatases (Ppp3Ca, Ppp2r1a, and
264 Ppp2r2b).

265 To infer functional interactions of the 125 BAR-PSER129 identified proteins we
266 performed Search Tool for the Retrieval of Interacting Genes/Proteins (STRING) analysis with
267 Markov Clustering (MCL). Results show 11 clusters of high confidence (>0.7) functional
268 interactions (Fig. 6D). The function of each interaction cluster was determined and annotated
269 using enrichment analysis. The largest functional cluster consisting of 18 proteins, including the
270 target protein alpha-synuclein, was enriched for "Presynaptic Vesicle Cycle / Glutamate". Other
271 clusters included "Fatty Acid Beta Oxidation", "Oxidative Phosphorylation/Parkinson's disease",
272 "Protein Kinase Binding", "Glycolysis", "Proton Transporting ATPase", "14-3-3 Domain", "Peptidyl-
273 serine Dephosphorylation", "Chaperonin-containing T-Complex", "mRNA Binding and Splicing",
274 and "Translation Factors." Enrichment analysis of the 125 identified proteins confirmed an overall
275 strong enrichment for presynaptic vesicle processes (False discovery rate (FDR) < $1x10^{-10}$ *SI*
276 *Appendix* Dataset S4 and S5) and 12 of the proteins identified were from the Kyoto Encyclopedia
277 of Genes and Genomes (KEGG) Parkinson's disease pathway. Several BAR-PSER129 identified
278 proteins (24/125) and functional clusters (5/11) identified here contained previously identified
279 alpha-synuclein interactors (25) (Fig. 6D, Open-circle nodes) while the remaining were distinct.

280 **Mitral cell PSER129 localizes with Ywhag**

281 BAR-PSER129 identified several 14-3-3 proteins, of which, Ywhag had been previously
282 found in close association with Lewy pathology and interacts with alpha-synuclein (26, 27).
283 Furthermore, Ywhag binds phosphoserine motifs raising the possibility that Ywhag directly
284 interacts with PSER129. To verify the BAR identified interaction between Ywhag and PSER129
285 we characterize the spatial association of both proteins in the healthy mouse brain. Results
286 showed that Ywhag was expressed in mitral cell layer (Fig. 7A) and ubiquitously expressed
287 throughout the brain (Fig. 7B). Brain regions with high PSER129 content often had high Ywhag
288 content (Fig. 7B, Yellow color shows overlap) but the overlap was not complete and several brain
289 sections, particularly in the cerebellum, overlap was rare. Brain regions previously found to have
290 high PSER129 content (Fig. 1A, C) were found to have overlapping Ywhag, with high overlap in
291 the dentate gyrus, accessory olfactory bulb, and substantia nigra reticulata (Fig. 7C).

292 In the OB, mitral cells and their apical dendrites were intensely labeled for Ywhag while
293 other OB layers showed moderate staining (Fig. 7D). Colocalization analysis of PSER129 positive
294 mitral cells revealed that PSER129-Ywhag association was variable from cell-to-cell and between
295 cellular compartments (Fig 7D). Within the mitral cell apical dendrites colocalization was
296 consistently observed. However, in the soma and nucleus the PSER129-Ywhag interaction was
297 variable between cells, with mitral cells in two mice showing negative correlation in these
298 compartments (Fig. 7E).

299 **PSER129 positive mitral cells are cfos negative**

300 The endogenous function of PSER129 remains unknown, but alpha-synuclein has been
301 consistently implicated in playing a role with cellular vesicle processes(25, 28). Several lines of
302 evidence suggest that neuronal activity might drive alpha-synuclein accumulation and potentially
303 phosphorylation(29, 30). Indeed alpha-synuclein may have SNARE functions, and neuronal
304 activity depolarization could drive accumulation/phosphorylation as SNARE becomes more
305 active. To test this hypothesis, we used multiplex TSA to label PSER129 and the immediate early
306 gene product AP-1 Transcription Factor Subunit (c-Fos) in the OB of WT mice. Nuclear c-Fos
307 expression increases with periods of intense neuronal depolarization/activity and therefore has
308 been used as a marker of recent neuronal activity. Results showed widespread nuclear c-Fos
309 expression throughout the layers of the OB, including the mitral cell layer (Fig. 8A,B). High
310 magnification images of the mitral cell layer (Fig. 8C) revealed that PSER129 positive mitral cells
311 lacked nuclear c-Fos expression. Cytosolic c-Fos was observed in PSER129 positive mitral cells,
312 but the biological significance of cytosolic c-Fos is unclear. In all the animals assessed (n=4), we
313 were unable to locate a single clear instance of a PSER129 positive mitral cell expressing nuclear
314 c-Fos.

315 **Discussion**

316 **Mitral cells in synucleinopathies**

317 The OB has been hypothesized to be one potential starting point for alpha-synuclein
318 pathology and therefore the synucleinopathy disease process (1, 11). This contention is
319 supported by several observations including 1) mitral cell loss in PD OB (2, 5, 18, 31), 2) high-
320 incidence of LP in synucleinopathy OB (3, 5, 32-34) 3) and incidental LP in OB (3). Our
321 inadvertent observation of PSER129 (which is usually associated with disease) in healthy mitral
322 cells seems to support this hypothesis. However, it seems unlikely that healthy mammalian mitral
323 cells harbor disease-causing aggregates, but instead the phosphorylation of alpha-synuclein
324 likely has a yet undefined biological role in mitral cells. BAR-PSER129 labeling identified
325 presynaptic vesicle machinery, fatty acid oxidation, mitochondrial oxidative phosphorylation,
326 glycolysis, and mRNA binding and splicing as being associated with PSER129 in the OB, which is
327 largely consistent with the known about the function and interactome of PSER129 (25, 27, 35).

328 Perturbations of these functionalities might contribute to the intracellular accumulation of
329 PSER129. Alternatively, aggregates of misfolded alpha-synuclein might inhibit one of these
330 functionalities resulting in accumulation and hyperphosphorylation of alpha-synuclein. Recently
331 evidence of this was observed following alpha-synuclein pathology induction in the OB of non-
332 human primates which subsequently suppressed glycolytic functions (36), suggesting that
333 aggregates are suppressing glycolysis which we found to be functionally associated with
334 PSER129. Factors such as normal aging that converge on cellular pathways identified here are
335 likely to have particular significance for mitral cell alpha-synuclein pathology and olfactory
336 function (5, 37).
337 PSER129 was closely, but not precisely, localized with PK-resistant alpha-synuclein in
338 the mouse OB. PK-resistance for alpha-synuclein occurs within pathological aggregates and via
339 alpha-synuclein-lipid interactions (38). Because we found evidence that PSER129 was
340 associated with cellular vesicle machinery (Fig. 6D) and apparently monomeric on SDS-PAGE
341 (Fig. 1E), the observed PK-resistant alpha-synuclein is likely due to lipid-alpha-synuclein
342 interactions and not aggregation. In agreement with this interpretation PSER129 was also not
343 associated with ubiquitin in mitral cells and therefore PK-resistant alpha-synuclein observed are
344 likely not toxic accumulations or oligomers that mitral cells are unable to clear. Interestingly, if
345 alpha-synuclein PK resistance in mitral cells is driven by lipid interactions, then PSER129 is only
346 proximally associated (i.e., lipid free) suggesting that phosphorylation is a cellular signaling event
347 that occurs prior to or following lipid-alpha-synuclein interactions, opening the possibility that
348 PSER129 is a “molecular switch” for lipid/vesicle interactions(39). Interestingly, we found
349 evidence that PSER129 positive mitral cells were inactive (i.e., cFos negative) which does not
350 support the hypothesis that neuronal activity is driving PSER129 and PK-resistance (i.e.,
351 lipid/vesicle interactions) (29, 30).
352 Our data is consistent with a scenario which has previously been suggested where LP
353 begins to form in the OB and then propagates to other brain regions in a prion-like fashion (1, 11).
354 Mitral and tufted cells have a apical dendrite that extends to a single glomerulus but they also
355 extend several axons into telencephalon regions including the amygdala (40). These axons
356 extend out through the olfactory tract. We observed occasional LP in the mitral cell layer of DLB
357 and PD OB, but consistently saw dense Lewy neurites throughout the anterior olfactory nuclei of
358 the main bulb and peduncle. In WT mice, brain regions known to be susceptible to LP in human
359 disease frequently displayed PSER129 immunoreactivity. Notably, the PSER129 distribution that
360 we observed here largely mirrored the known high abundance of alpha-synuclein in glutamatergic
361 presynaptic nerve terminals in the healthy mouse brain (41, 42). If PSER129 containing brain
362 regions are normally susceptible to pathology formation (43), then our observations corroborates
363 a hypothesis that olfactory cortex projections are the primary pathogenic origin of

364 synucleinopathies (31, 32, 34, 44-46) and perhaps insults like excitotoxicity in the OB (47, 48)
365 initiate the pathological processes. Similarly, if misfolding/seeding probabilities are a function of
366 local alpha-synuclein concentration (49), then glutamatergic processes are a high-probability site
367 for disease initiation. Aggravating factors like Infection (viral or bacterial) via nasal cavity (1) might
368 promote alpha-synuclein accumulation (50) and preferentially initiate the pathological process in
369 susceptible mitral cells.

370 Recent reports looking at Lewy pathology distribution in PD described cases where OB
371 was not present and (51-53). Two PD subtypes might exist where pathology begins either in the
372 peripheral nervous system “body-first” or in the central nervous system “brain-first”, with Lewy
373 pathology being brain-stem prominent or OB prominent, respectively(51-53). We observed
374 apparent Lewy pathology (PK-resistant PSER129 reactivity) in all human PD OBs tested here,
375 however the sample size is small. Therefore, we cannot make definitive conclusions about Lewy
376 pathology distribution in the synucleinopathy OB. We can conclude that Lewy pathology occurs in
377 mitral cell layer as observed by others(54) and in the non-synucleinopathy OB PSER129
378 reactivity can be detected in mitral cells. Future studies should assess larger human sample
379 cohorts to provide in depth characterization of Lewy pathology in the OB.

380 We initiated the present study because we had observed regionally specific anomalous
381 PSER129 signal in healthy WT mice. Interestingly others have previously observed this mitral
382 cell-staining phenomenon but did not emphasize its potential importance to our understanding of
383 synucleinopathies (55) and the mitral cell PSER129 signal has been often dismissed as
384 “background.” We demonstrated that the anomalous PSER129 signal was sensitive to PK
385 digestion. In mitral cells both diffuse and punctate structures were intensely labeled in the
386 nucleus, cytoplasm, and often observed throughout their apical dendrite. The apparent pattern of
387 PSER129 staining was seen in mice, rats, non-human primates, and a neurologically intact
388 human. This suggest the role of PSER129 in OB mitral cells is conserved across mammalian
389 species. However, mitral cell PSER129 reactivity was not universal, as we did not observe any
390 PK-sensitive PSER129 staining in 1 mouse and 3 healthy humans. This suggests that either
391 PSER129 is generated in mitral cells driven by fluctuating cellular process or the PSER129
392 epitope is not accessible/preserved in some tissues. We explored many epitope retrieval methods
393 and found that heat mediate epitope retrieval enhanced reactivity but did not unmask reactivity in
394 samples that showed no PSER129 reactivity to begin with, suggesting that hidden PSER129
395 epitopes are not responsible. In mice, we observed an “all-or-none” phenomenon where samples
396 with little/no OB staining also had little/no staining in other brain regions. The exact reason for this
397 phenomenon remains unclear. However, we found PSER129 interactions were strongly enriched
398 for presynaptic glutamatergic vesicle processes, and therefore fluctuations in these processes or
399 related calcium influx (56) could be driving the observed PSER129 in mitral cells. Alternatively, a

400 recent report found that tandem PTM's of alpha-synuclein PSER129 prevent detection by
401 EP1536Y (20) and therefore further modification of PSER129 might account for the observed loss
402 of PSER129 signal in some brains. Postmortem, dephosphorylation of PSER129 occurs rapidly in
403 brain tissue lysates (15) and this might account for the lack of endogenous PSER129 in non-
404 synucleinopathy post-mortem human brain samples. Indeed, the only non-synucleinopathy
405 human OB sample to show an endogenous PSER129 signal had the shortest PMI of specimens
406 tested here (Sample #30, PMI = 3.08 h)
407 In agreement with previous reports, results from our studies show that improper dilution
408 of EP1536Y results in abundant off target binding as determined by IHC and blotting techniques
409 (Figure S1,B). In contrast to previous reports, we demonstrate that endogenous PSER129 is
410 detectable provided EP1536Y is highly dilute, and the secondary detection system is sufficiently
411 sensitive (in this case TSA). In our hands, we found much lower concentrations of EP1536Y than
412 commonly used (Abcam) are necessary to ensure on target binding, and commonly employed
413 dilutions have a high probability of generating false positive detection. In our hands, EP1536Y
414 could be diluted to ~3 pg / mL (1:1,000,000 dilution) and still show on target staining. This gives a
415 large window of effective concentrations for this antibody, as we also observed that non-specific
416 binding is eliminated somewhere between 1:10K and 1:20K dilutions (Fig S1, B).
417 Synucleinopathy has not been observed as a function of aging in mammals besides
418 humans for unknown reasons. By contrast, lesions resembling human tau tangles and amyloid
419 plaques have been observed in mammals other than humans (57). In the mouse OB, we found
420 disease associated phosphorylated tau was restricted to fibers in the glomerular, inner plexiform
421 and outer nerve layers, but was not observed in mitral cells (*Si Appendix* Fig. S9). The human OB
422 is unique amongst mammals in several aspects including that it only exhibits limited post-natal
423 neurogenesis(57). Human samples had the least prominent PSER129 staining of all species
424 tested (Figure 3A). One possibility is that PSER129 represents a protective mechanism that
425 prevents pathological aggregation (58) and perhaps human mitral cells are particularly deficient in
426 this neuroprotective phosphorylation event as they age.
427
428 **Study Limitations**
429 Studies herein are based on antibody affinity, and although we have included multiple
430 controls (i.e., alpha-synuclein knockout mice, antibody preabsorbtion, primary antibody negative
431 conditions, and WB with phosphatase treatment) we cannot completely rule out the possibility of
432 immune mimicry(17). However, our finding that under several IHC protocols tested (e.g., HIAR,
433 PK), we did not observe any PSER129 immunoreactivity in any brain structure of seven alpha-
434 synuclein knockout mice. In contrast, nearly all (14/15) of the WT mice tested had readily
435 apparent immunoreactivity in the OB mitral layer. Using WB, we found that EP1536Y reacts to a

436 single 15-kDa species that is abolished by phosphatase pretreatment, and not observed in alpha-
437 synuclein KOs, consistent with detection of PSER129 (Figure 1E,F). Furthermore, BAR-PSER129
438 capture samples were enriched for alpha-synuclein as confirmed by both immunoblotting and LC-
439 MS/MS identification (Figure 4). Together, these observations make immune mimicry very
440 unlikely. A second limitation of the current study is the relatively small number of human OB
441 assessed here.

442 **Conclusion**

443 PSER129 accumulates in OB mitral cells of healthy mammals and interacts
444 predominantly with presynaptic vesicle components. Determining the molecular and cellular
445 factors driving the transition from endogenous PSER129 to accumulation of abnormal PSER129
446 in the OB mitral cells will provide important insights into the origins of synucleinopathies.
447

448 **Materials and Methods**

449 **Biological Specimens**

450 All rodent and non-human primate tissues were derived from studies conducted in
451 accordance with institutional IACUC approved protocols. All animals were anesthetized
452 (ketamine/xylazine for rodents, and ketamine/xylazine/hydromorphone for non-human primates)
453 and transcardially perfused with PBS pH 7.4 followed by 4% paraformaldehyde (PFA) in PBS.
454 Collected brain tissues were post fixed in 4% PFA in PBS overnight at 4°C, dehydrated in
455 successive sucrose solutions in PBS (i.e.,10%, 20%, and 30% sucrose, w/v), and cut into 40-
456 micron coronal sections on a freezing stage microtome. Human OB from individuals clinically
457 diagnosed with PD were supplied by the Rush Movement Disorders Brain Bank. OB specimens
458 from individuals without synucleinopathy (HC) were provided by Rush Alzheimer's Brain Bank
459 and BH Banner Health Research. Human and non-human primate OBs were sectioned following
460 embedding in optimal cutting temperature (O.C.T.) compound (ThermoFisher). One human non-
461 synucleinopathy case was obtained from banner health embedded in paraffin wax (Specimen
462 details see Table 1 and *SI Appendix* Table S1). Paraffin embedded sections were heated in an
463 oven to 60°C, cleared with xylenes, and rehydrated with successive ethanol solutions from 100%
464 to 50% prior to IHC. Once hydrated sections were processed according to immunostaining
465 protocols.

466 **Immunohistochemistry**

467 Free floating PFA fixed mouse sections gathered at intervals of 940 microns across the
468 neuroaxis (i.e., OB to brainstem) were first incubated in peroxidase quenching solution (0.3%
469 hydrogen peroxide, 0.1% sodium azide) in TBST (50 mM Tris-HCl pH 7.6, 150mM NaCl, and
470 0.5% Triton X-100) for 30 min at room temperature. Sections were then rinsed twice with PBS
471 and incubated with blocking buffer (3% normal serum, 2% BSA, TBST) for 1 h at room

472 temperature. Sections were then incubated with either PSER129 antibody (Abcam, “EP1536Y”)
473 diluted 1:50,000, TBX21 antibody (Santa Cruz Biotechnology) diluted 1:10,000, cfos antibody
474 (Abcam) diluted 1:10,000, Ywhag antibody (Abcam) diluted 1:5,000, alpha-synuclein antibody
475 (Abcam, “EPR20535”) diluted 1:10,000, ubiquitin antibody (Abcam) 1:10,000 diluted in blocking
476 buffer overnight at 4°C. The next day sections were washed twice with TBST and incubated with
477 biotinylated anti-rabbit or anti-mouse antibodies (Vector Laboratories) diluted 1:200 in blocking
478 buffer for 1h at room temperature. Sections were then wash 3 times for ten minutes each in TBST
479 and then incubated with prepared elite avidin biotin complex (ABC) reagent (Vector Laboratories)
480 for 1 h at room temperature. Sections were then washed 2 times for 10 min in TBST and then
481 washed 2 times for 10 min in sodium borate buffer (0.05M Sodium Borate, pH 8.5). Sections were
482 then incubated 30 min with 1 µg / mL biotinyl tyramide (Sigma-Aldrich) and 0.003% hydrogen
483 peroxide diluted in sodium borate buffer. Then sections were washed 3 times for 10 min in TBST
484 and incubated again in the previously prepared elite ABC reagent for 1 h at room temperature.
485 Sections were then washed 3 times for 10 min in TBST. Sections were then developed using a
486 standard nickel enhanced 3,3'-diaminobenzidine (DAB)-imidazole protocol. Mounted sections
487 were counterstained with methyl green, dehydrated with ethanol, cleared with xylenes, and
488 coverslipped with cytoseal 60 (Fisher Scientific).
489 For some experiments, sections were digested with PK (Thermofisher Scientific) prior to
490 IHC. These sections were first mounted onto gelatin-coated slides, dried, and baked overnight at
491 55°C. Slides were then placed into PBS for 10 min and then PK digestion buffer (TBS, 0.1% triton
492 X100, 20 µg PK / mL, warmed to 37°C) for 20 min. Sections were rinsed with PBS, incubated with
493 4% PFA for 10 min, and rinsed off twice with TBST. Digested sections were then processed as
494 stated above. For some experiments heat induced antigen retrieval (HIAR) was performed prior
495 to staining. To perform HIAR citrate buffer (10mM sodium citrate, 0.05% Tween 20, pH 6.0) was
496 heated in a water bath to 90°C, slides then immersed in this solution for 30 min, and then allowed
497 to cool to room temperature.
498 **TSA Multiplex Labeling**
499 IHC was performed as described above with the exception that CF-488, CF-568 or CF-
500 647 tyramide conjugates (Biotium) were substituted for biotinyl tyramide at a final concentration of
501 1 µg / mL. Multiplex labeling was performed by heating samples 90°C for 30 min in citrate buffer
502 to remove the antibody complex following the tyramide reaction like what has been previously
503 described (59, 60). TSA multiplex labeling of PSER129 and PK-resistant alpha-synuclein was
504 achieved by first labeling PSER129 with CF-568-tyramide. Samples were then heated in citrate
505 buffer as described above, then allowed to cool. Samples were then washed with TBST and
506 incubated for 3 minutes at 37°C with PK digestion buffer with or without 20 µg PK / mL. Samples
507 were then placed in 4% PFA for 10 min and then washed with TBST. Fluorescently labeled

508 sections were mounted onto gelatin-coated slides, dried for 20 min, and covered with #1.5 glass
509 coverslip using FluoroShield mounting medium (Sigma-Aldrich).
510 **BAR-PSER129**
511 Free-floating PFA fixed mouse OB sections gathered at intervals of 120 microns were
512 processed as described above and previously (24). Each sample consisted of ~15-20 OB tissue
513 sections. Sections from WT and alpha-synuclein KO mice were used. Capture conditions were
514 conducted both with primary antibody (i.e., EP1536Y) and without primary antibody. Following the
515 biotinyl tyramide reaction sections were washed overnight in PBS, and then heated to 98°C in
516 1mL of crosslink reversal buffer (500mM Tris-HCl pH 8.0, 5% SDS, 150mM NaCl, and 2mM
517 EDTA) for 30 min. Samples were then vortexed vigorously, heated for an additional 15 min, and
518 centrifuged for 30 min at 22,000 x g. The supernatant was diluted 1:10 in dilution buffer (50mM
519 Tris-HCl pH 8.0, 1% triton X-100, 150mM NaCl) and incubated with 25 micrograms of streptavidin
520 magnetic beads (ThermoFisher Scientific) overnight at 4°C with nutation. The following day,
521 beads were collected on a magnetic stand, washed 3 times for 1 h each with wash buffer (50mM
522 Tris-HCl pH 8.0, 1% triton X-100, 0.1% SDS, and 150mM NaCl), and then 1 time with TBST for 1
523 h. Beads were then collected and boiled in 40 microliters sodium dodecyl sulfate polyacrylamide
524 gel electrophoresis (SDS-PAGE) sample buffer containing 5% beta-mercaptoethanol for 10 min
525 and mixed vigorously. 38 µl were run a distance of ~1 cm into an SDS-PAGE gel (Fisher
526 Scientific), the gel was fixed (1 h in 50% ethanol, 10% acetic acid), stained with coomassie blue,
527 and entire lane excised for subsequent trypsin digestion and Liquid chromatography tandem
528 mass spectrometry (LC-MS/MS).
529 **LC-MS/MS**
530 Gel bands were washed in 100 mM ammonium bicarbonate (AmBic)/acetonitrile (ACN)
531 and reduced with 10 mM dithiothreitol at 50°C for 45 minutes. Cysteines were alkylated with 100
532 mM iodoacetamide in the dark for 45 minutes at room temperature (RT). Gel bands were washed
533 in 100 mM AmBic/ACN prior to adding 1 µg trypsin (Promega #V5111) for overnight incubation at
534 37°C. Supernatant containing peptides were collected into a new tube. Gel pieces were washed
535 with gentle shaking in 50% ACN/1% FA at RT for ten minutes, and supernatant was collected in
536 the previous tubes. Final peptide extraction step was done with 80% ACN/1% FA, and 100%
537 ACN, and all supernatant was collected. The peptides were dried in a speedvac and reconstituted
538 with 5% ACN/0.1% FA in water before injecting into the LC-MS/MS.
539 Peptides were analyzed by LC-MS/MS using a Dionex UltiMate 3000 Rapid Separation
540 nanoLC coupled to an Orbitrap Elite Mass Spectrometer (Thermo Fisher Scientific Inc.). Samples
541 were loaded onto the trap column, which was 150 µm x 3 cm in-house packed with 3 µm
542 ReproSil-Pur® beads. The analytical column was a 75 µm x 10.5 cm PicoChip column packed
543 with 3 µm ReproSil-Pur® beads (New Objective, Inc. Woburn, MA). The flow rate was kept at 300

544 nL/min. All fractions were eluted from the analytical column at a flow rate of 300 nL/min using an
545 initial gradient elution of 5% B from 0 to 5 min, transitioned to 40% over 100 min, 60% for 4 mins,
546 ramping up to 90% B for 3 min, holding 90% B for 3 min, followed by re-equilibration of 5% B at
547 10 min with a total run time of 120 min. Mass spectra (MS) and tandem mass spectra (MS/MS)
548 were recorded in positive-ion and high-sensitivity mode with a resolution of ~60,000 full-width
549 half-maximum. The 15 most abundant precursor ions in each MS1 scan were selected for
550 fragmentation by collision-induced dissociation (CID) at 35% normalized collision energy in the
551 ion trap. Previously selected ions were dynamically excluded from re-selection for 60 s. The
552 collected raw files spectra were stored in .raw format.
553 Proteins were identified from the MS raw files using the Mascot search engine (Matrix
554 Science, London, UK. version 2.5.1). MS/MS spectra were searched against the SwissProt
555 mouse database. All searches included carbamidomethyl cysteine as a fixed modification and
556 oxidized methionine, deamidated asparagine and aspartic acid, and acetylated N-terminal as
557 variable modifications. Biotin (K), Biotin(N-term) were set as a variable modification for
558 biotinylation detection. Three missed tryptic cleavages were allowed. A 1% false discovery rate
559 cutoff was applied at the peptide level. Only proteins with a minimum of one peptides above the
560 cutoff were considered for further study. Identified peptides/protein were visualized by Scaffold
561 software (version 5.0, Proteome Software Inc., Portland, OR).
562 **Pathway Analysis**
563 Full STRING network analysis was conducted on the 125 PSER129-interacting proteins
564 identified by BAR. For STRING, protein identifiers minimum required interaction score was set to
565 0.7 (i.e. high confidence) and singlet nodes (i.e. no interactions) were discarded by selecting
566 “hide disconnected nodes in the network”. Data for all functional and physical protein associations
567 were used. Resulting STRING network was exported to cytoscape v.3.9.1 for Markov Cluster
568 Algorithm (MCL) clustering and pathway analysis. Consensus terms for each cluster was
569 determined by gene ontology (GO) most enriched pathways (i.e., lowest FDR). The final
570 annotated interaction map was manually compared with alpha-synuclein interactions previously
571 identified *in vivo* using proximity labeling methods (25).
572 **Spot Blotting**
573 Prior to MS, 1 µl of streptavidin bead eluent was spotted onto a methanol activated
574 polyvinylidene difluoride (PVDF) membrane and allowed to dry completely. The membrane was
575 then reactivated in methanol, washed in water, and post-fixed in 4% PFA for 30 min. Blots were
576 then rinse with TBST (20mM Tris-HCl pH 7.6, 150mM NaCl, 0.1% Tween-20) and placed in
577 blocking buffer (TBST and 5% BSA) for 1 h at room temperature. To detect biotinylated proteins,
578 blots were incubated with ABC (VectorLabs) diluted 1:10 in blocking buffer for 1 h at room
579 temperature. To detect alpha-synuclein blots were incubated overnight with SYN1 diluted 1:2,000

580 in blocking buffer, washed, and then incubated with anti-mouse HRP conjugate diluted 1:6,000 in
581 blocking buffer (Cell Signaling). All membranes were washed in high stringency wash buffer
582 (20mM Tris-HCl pH 7.6, 400mM NaCl, 0.1% Tween-20) and imaged using enhanced
583 chemiluminescence (ECL) substrate (Biorad, product # 1705060) and Chemidoc imager (Biorad).

584 **Western Blotting**

585 Proteins were extracted from unlabeled fixed floating tissue sections as described above.
586 Extracted proteins were precipitated by chloroform-methanol (61) and re-dissolved in 5% SDS.
587 Protein concentrations were determined using bicinchoninic acid assay (BCA, ThermoFisher) and
588 20 micrograms of total protein was separated on 4-12% Tris-glycine gel. Proteins were blotted
589 onto PVDF membranes, membranes were then post-fixed with 4% PFA for 30 min, dried, and
590 reactivated in methanol for immunoblotting. Membranes incubated 1 h in blocking buffer (TBST
591 with 5% non-fat milk, 0.5% polyvinylpyrrolidone) and then with either SYN1 (diluted 1:2,000) or
592 PSER129 (diluted 1:20,000) antibodies diluted in blocking buffer overnight at 4°C. The following
593 day membranes were washed 3 X 10 min in TBST and incubated with anti-rabbit (Invitrogen,
594 1:20,000) or anti-mouse (Cell Signaling, 1:6,000) HRP conjugates for 1 h at room temperature.
595 Membranes were then washed 3 X 10 min in TBST. Membranes were imaged using ECL
596 substrate and chemiluminescence imager (Biorad). 5 microliters of a broad range molecular
597 weight standard (Biorad, product # 1610394) was used to determine approximate molecular
598 weight of separated proteins

599 **Calf Intestine Alkaline Phosphatase (CIAP) treatment**

600 Proteins were separated and blotted as described above. All samples to be tested were
601 loaded in duplicate on the same gel and blotted to the same membrane. Following PFA fixation,
602 membranes were stained with ponceau S and cut to separate the duplicates. Both membranes
603 were blocked as previously described, and then washed 3 X 5 min with TBST. One blot was
604 incubated at 37°C for 2h with 10mL CIAP buffer (100mM NaCl, 10mM MgCl2, and 50mM Tris-
605 HCl pH 7.9) containing 1000 units CIAP enzyme (Promega) and the other blot was incubated with
606 CIAP buffer without CIAP enzyme. Blots were then washed 3 x 5 min with TBST and
607 immunoprobed as described above. Blots were imaged in tandem.

608 **Microscopy**

609 All samples were imaged on an inverted confocal microscope (Nikon A1R). Whole slide
610 bright-field images using a 4X or 10X objective were acquired for DAB labeled sections. Confocal
611 images were acquired for fluorescently labeled sections using a 60X oil immersion objective.
612 Deconvolution of confocal images and colocalization analysis was performed using Nikon
613 elements software. Colocalization data was plotted using Prism (GraphPad Software).

614 **Acknowledgments**

Human brain samples were generously provided by several tissue banks including the Rush Movement Disorders Brain Bank and Rush Alzheimer's Disease Brain Bank. We are grateful to the Banner Sun Health Research Institute Brain and Body Donation Program of Sun City, Arizona for the provision of human olfactory bulb samples. The Brain and Body Donation Program is supported by the National Institute of Neurological Disorders and Stroke(U24 NS072026 National Brain and Tissue Resource for Parkinson's Disease and Related Disorders), the National Institute on Aging (P30 AG19610, Arizona Alzheimer's Disease Core Center), the Arizona Department of Health Services (contract 211002, Arizona Alzheimer's Research Center), the Arizona Biomedical Research Commission (contracts 4001,0011,05-901 and 1001 to the Arizona Parkinson's Disease Consortium) and the Michael J. Fox Foundation for Parkinson's Research. Funding for this work was provided by NIDCD Award #R01DC06519 (PB and GM) and NINDS Award #5R21NS109871-02 (JHK). Proteomics services were performed by the Northwestern Proteomics Core Facility, generously supported by NCI CCSG P30 CA060553 awarded to the Robert H Lurie Comprehensive Cancer Center, instrumentation award (S10OD025194) from NIH Office of Director, and the National Resource for Translational and Developmental Proteomics supported by P41 GM108569. All postmortem human brain samples were collected with consent from institutional ethics committees.

Data Availability

All raw LC-MS/MS data is publicly available via Proteomics Identifications Database (PRIDE).

Figures and Tables

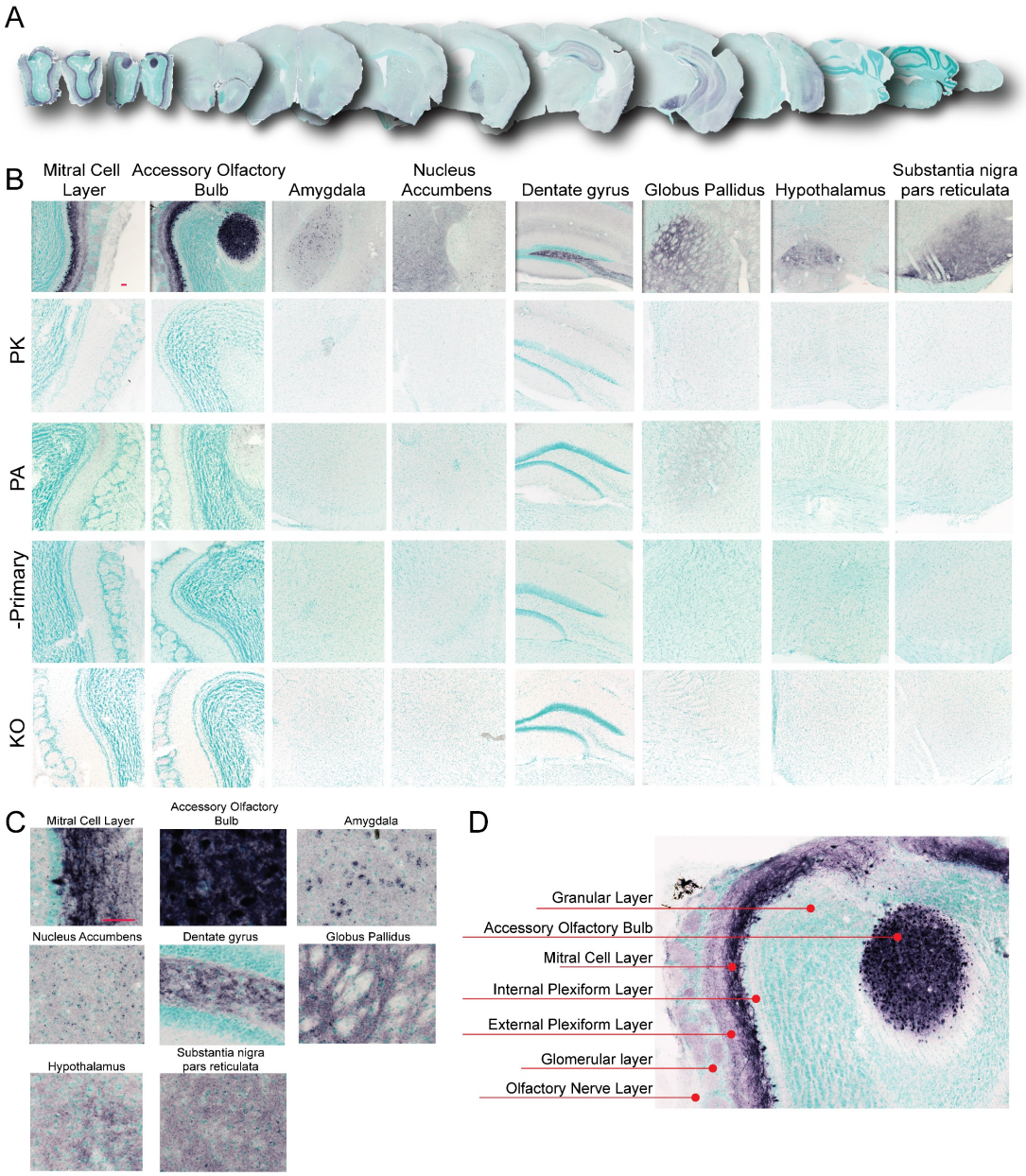
A
B
Mitral Cell Layer
Accessory Olfactory Bulb
Amygdala
Nucleus Accumbens
Dentate gyrus
Globus Pallidus
Hypothalamus
Substantia nigra pars reticulata
PK
PA
-Primary
KO
C
Mitral Cell Layer
Accessory Olfactory Bulb
Amygdala
Nucleus Accumbens
Dentate gyrus
Globus Pallidus
Hypothalamus
Substantia nigra pars reticulata
D
Granular Layer
Accessory Olfactory Bulb
Mitral Cell Layer
Internal Plexiform Layer
External Plexiform Layer
Glomerular layer
Olfactory Nerve Layer

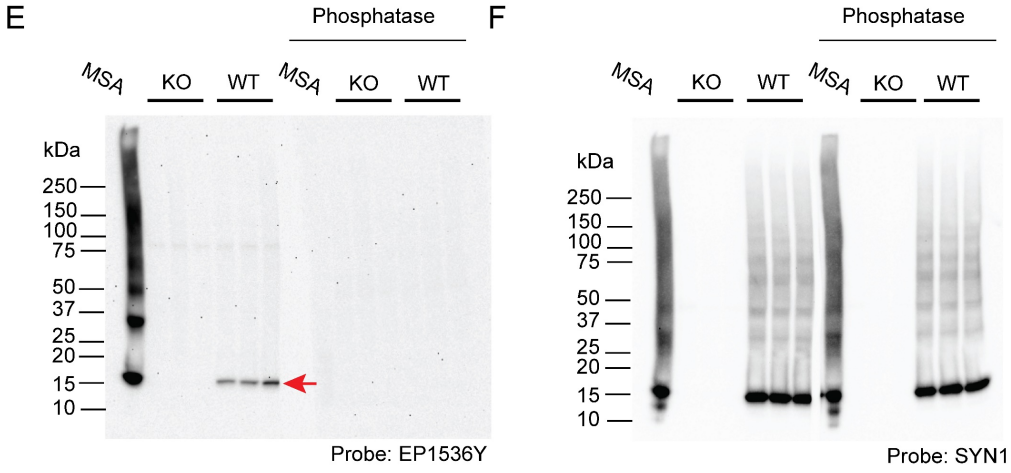
E
Phosphatase
MSA
KO
WT
MSA
KO
WT
kDa
250
150
100
75
50
37
25
20
15
10
Probe: EP1536Y
F
Phosphatase
MSA
KO
WT
MSA
KO
WT
kDa
250
150
100
75
50
37
25
20
15
10
Probe: SYN1

639 **Figure 1.** Distribution of PSER129 in the brain of non-diseased mice. (A) Coronal mouse brain
640 sections stained for PSER129 using TSA. (B) Representative images of select brain regions with
641 PSER129 immunoreactivity at high magnification. Tissues digested with PK, incubated with anti-
642 PSER129 antibody preabsorbed against PSER129 (PA), processed without primary antibody (-
643 Primary) and from mice lacking alpha-synuclein (KO). Representative images of select brain
644 regions are shown. Scale bars = 50 microns. WT mice, n = 14, KO mice, n = 7. (C) Enlarged
645 images from select brain regions showing PSER129 staining patterns in each region. (D)
646 Enlarged image from figure B, annotated to show the distribution of PSER129 across layers of
647 the OB. (E) Western blots of proteins extracted from the olfactory bulb of WT and KO mice
648 probed for PSER129. Blots were conducted in duplicate, with one blot being pretreated with
649 CIAP. (F) Blots reprobed for total alpha-synuclein (antibody “SYN1”). “MSA” denotes a positive
650 control sample. For “MSA,” 20 micrograms of protein extracted from a single striatal section of a
651 MSA brain was separated and blotted. Red arrow denotes a single 15 kDa PSER129 positive
652 band in WT OB. WT, n=3; KO, n=3.
653
654

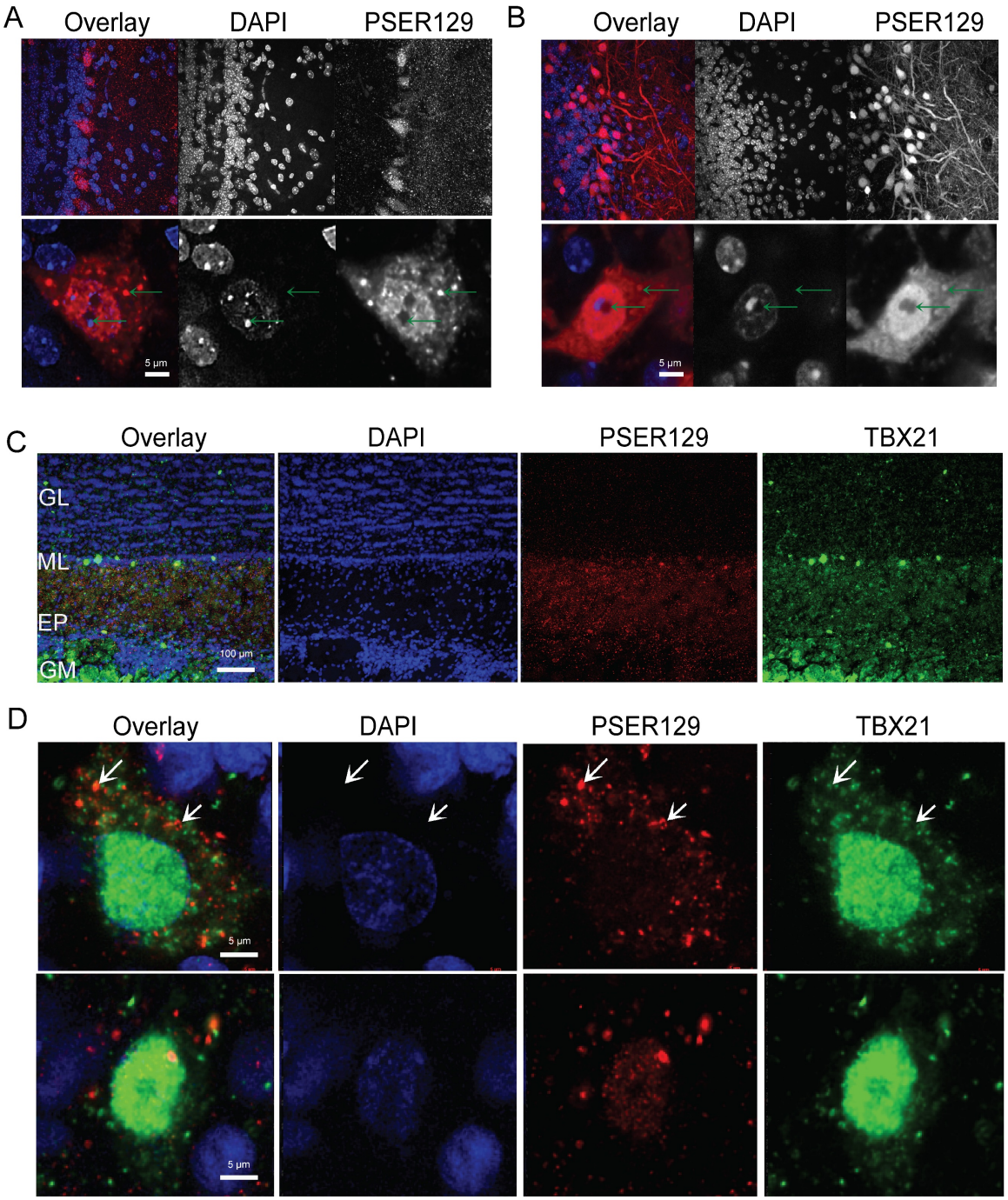

Figure 2. Localization and intracellular distribution of PSER129 in the non-diseased OB. (A) PSER129 was fluorescently labeled using tyramide signal amplification in WT mice. Tissues were counterstained with DAPI. Representative images showing distribution of PSER129 in the OB. (B) Non-pathology bearing M83 mice labeled for PSER129. Non-human primate OB was dual labeled

662 for PSER129 and mitral cell marker TBX21. (C) Low magnification confocal images showing
663 regional distribution in non-human primate OB. (D) High magnification confocal images showing
664 PSER129 puncta in TBX21 positive mitral cell. Green arrows denote intracellular punctate
665 structures, both perinuclear and nuclear. WT mice n=5, M83 mice n=2, non-human primates = 2,
666
667
668

669

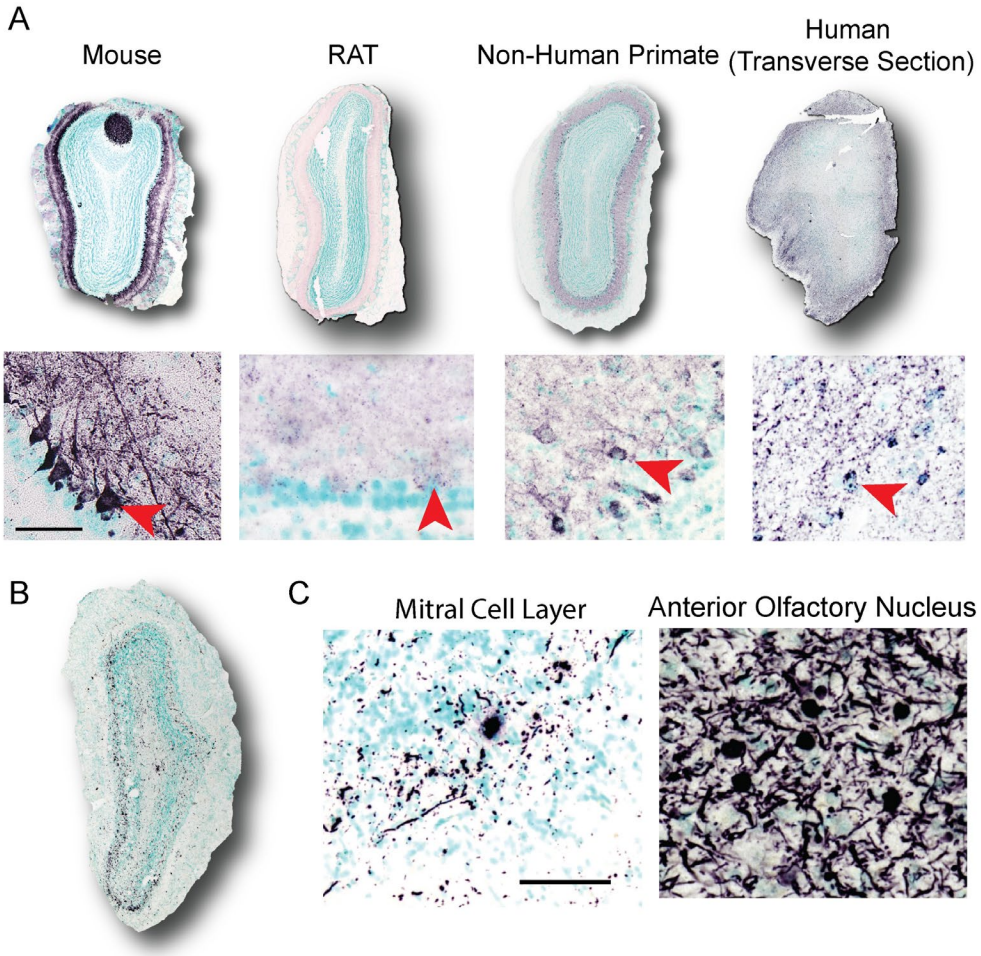

670
671
672
673 **Figure 3:** Mitral cell PSER129 is conserved across species (A) Representative images of
674 PSER129 staining in OB sections from mice, rat, non-human primate, and human. All sections
675 were coronal, except for human OB, which was section in the transverse plane. Depicted below
676 each olfactory bulb are high magnification images of staining in the mitral layer. Scale bar = 50
677 microns. Red arrowheads indicate positive PSER129 mitral cells. (B) Representative images of
678 PSER129 staining in PD/DLB OB. Section from the main bulb depicted. High magnification
679 images show PSER129 staining in the mitral cell layer and anterior olfactory nucleus. Scale bar =
680 50 microns.
681
682
683
684

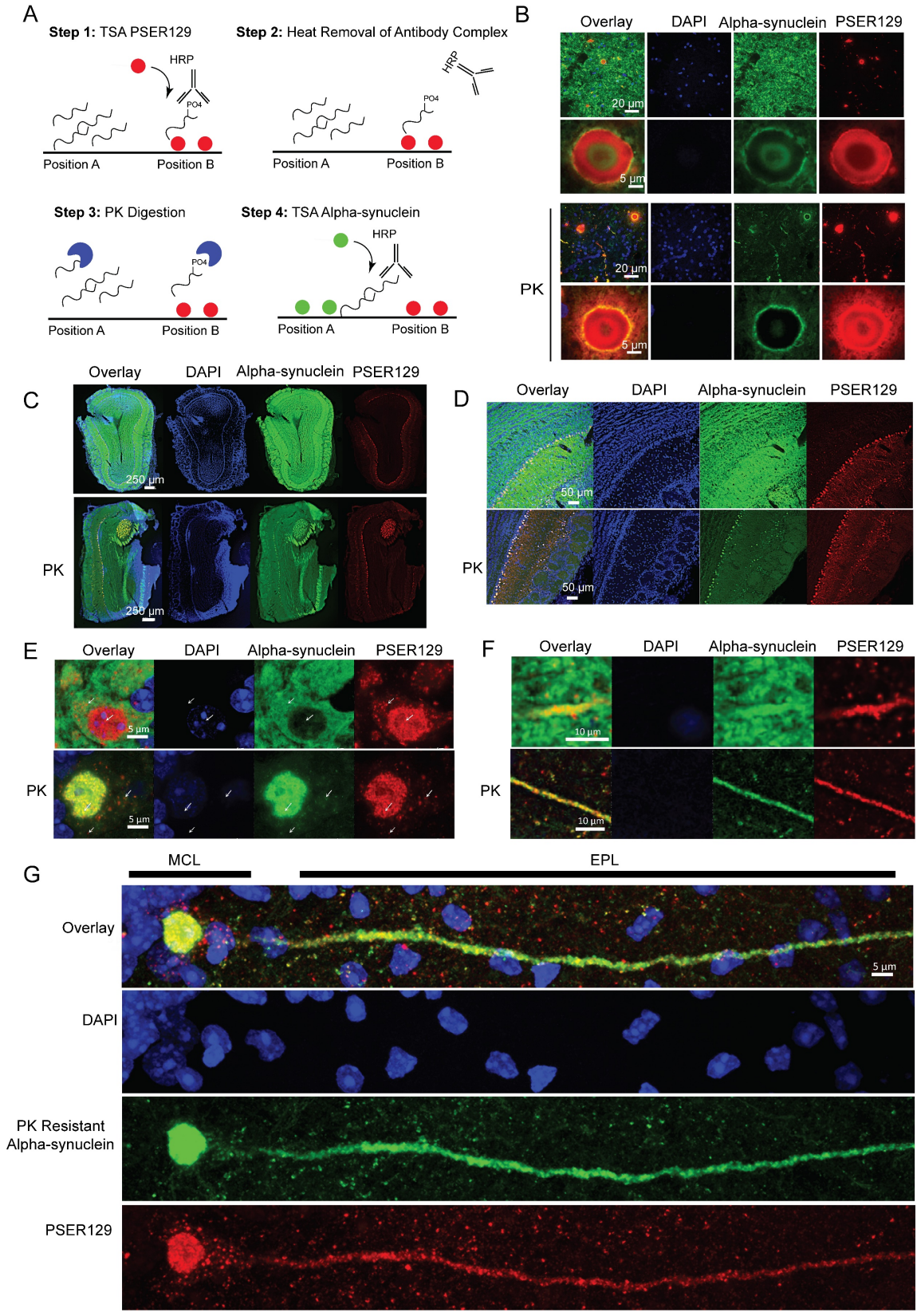
A
Step 1: TSA PSER129
HRP
PO4
Position A
Position B
Step 2: Heat Removal of Antibody Complex
HRP
PO4
Position A
Position B
Step 3: PK Digestion
PO4
Position A
Position B
Step 4: TSA Alpha-synuclein
HRP
Position A
Position B
B
Overlay
DAPI
Alpha-synuclein
PSER129
20 µm
5 µm
PK
20 µm
5 µm
C
Overlay
DAPI
Alpha-synuclein
PSER129
250 µm
PK
250 µm
D
Overlay
DAPI
Alpha-synuclein
PSER129
50 µm
PK
50 µm
E
Overlay
DAPI
Alpha-synuclein
PSER129
5 µm
PK
5 µm
F
Overlay
DAPI
Alpha-synuclein
PSER129
10 µm
PK
10 µm
G
MCL
EPL
Overlay
5 µm
DAPI
PK Resistant
Alpha-synuclein
PSER129

685

686 **Figure 4.** PSER129 associates with PK-resistant alpha-synuclein in the mouse OB. (A) Summary
687 of approach for measuring PK resistance in situ. Step 1, the location of PSER129 is labeled using
688 TSA. CF568 dye is covalently bound to tissue (Position “B”). Step 2, low pH and heat are used to
689 remove the antibody complex from the tissue while leaving the CF568 dye intact. Step 3, tissues
690 are briefly treated with PK to destroy enzyme accessible epitomes of alpha-synuclein. Step 4,
691 antibody against total alpha-synuclein is used for TSA labeling of remaining alpha-synuclein in
692 the sample. (Position “A”). Result allows simultaneous visualization of PK sensitive and PK
693 resistant epitopes. (B) PD brain sections processed with this dual-labeling protocol. High
694 magnification confocal images of the substantia nigra. Top panels depict results without PK and
695 below with PK digestion (“PK”). (C) Low magnification confocal images of OB dual-labeled for
696 PSER129 and alpha-synuclein. Top panels show an OB section processed in the absence of PK.
697 Bottom panels depict OB sections processed with PK. (D) High magnification images of the mitral
698 cell layer. Expanded high magnification images depicting a mitral cell body (E) and apical
699 dendrite (F) in the outer plexiform layer with (bottom panel) and without PK (top panel). (G)
700 Distribution of PSER129 and PK-resistant alpha-synuclein in a single OB mitral cell. (WT mice
701 n=3, PD substantia nigra = 3)

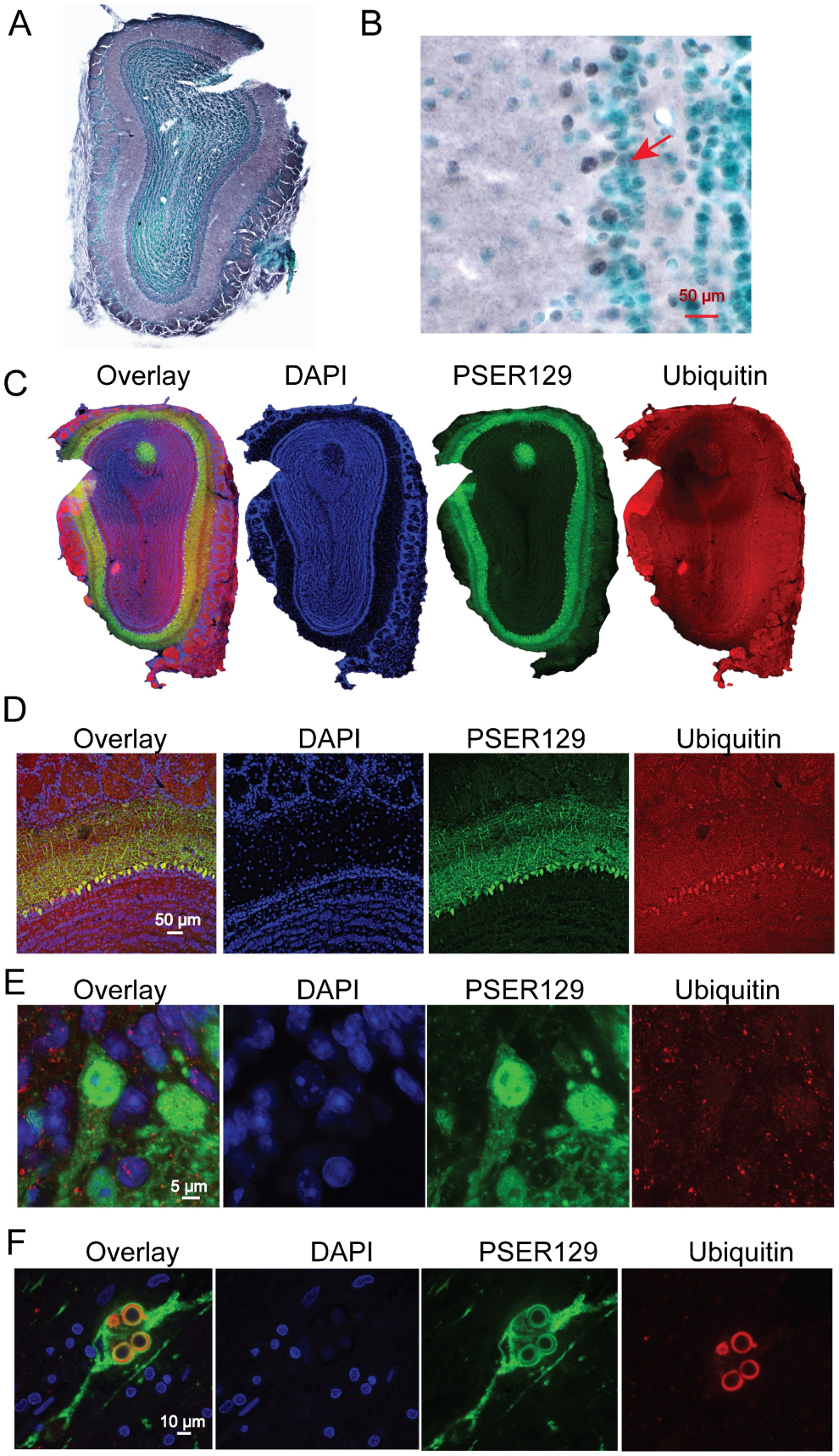
A
B
50 µm
C
Overlay
DAPI
PSER129
Ubiquitin
D
Overlay
DAPI
PSER129
Ubiquitin
50 µm
E
Overlay
DAPI
PSER129
Ubiquitin
5 µm
F
Overlay
DAPI
PSER129
Ubiquitin
10 µm

702

703 **Figure 5.** PSER129 is not associated with ubiquitin in OB mitral cells. Ubiquitin levels and
704 distribution in the mouse OB was determined. (A) Low magnification image showing ubiquitin
705 staining in the main OB. (B) High magnification image showing ubiquitin staining in the mitral cell
706 layer. Red arrow denotes ubiquitin positive cell in the mitral cell layer. (C) Low magnification
707 images of OB sections fluorescently labeled for PSER129 and ubiquitin. (D) High resolution
708 confocal images showing distribution of ubiquitin in the mitral cell layer. (E) Confocal image of
709 single PSER129 positive mitral cell. (F) Substantia nigra from PD brain fluorescently labeled for
710 ubiquitin and PSER129 using the same TSA multiplex approach. All sections counter stained with
711 either methyl green or DAPI (WT mice n=3, PD substantia nigra n=3).
712
713
714

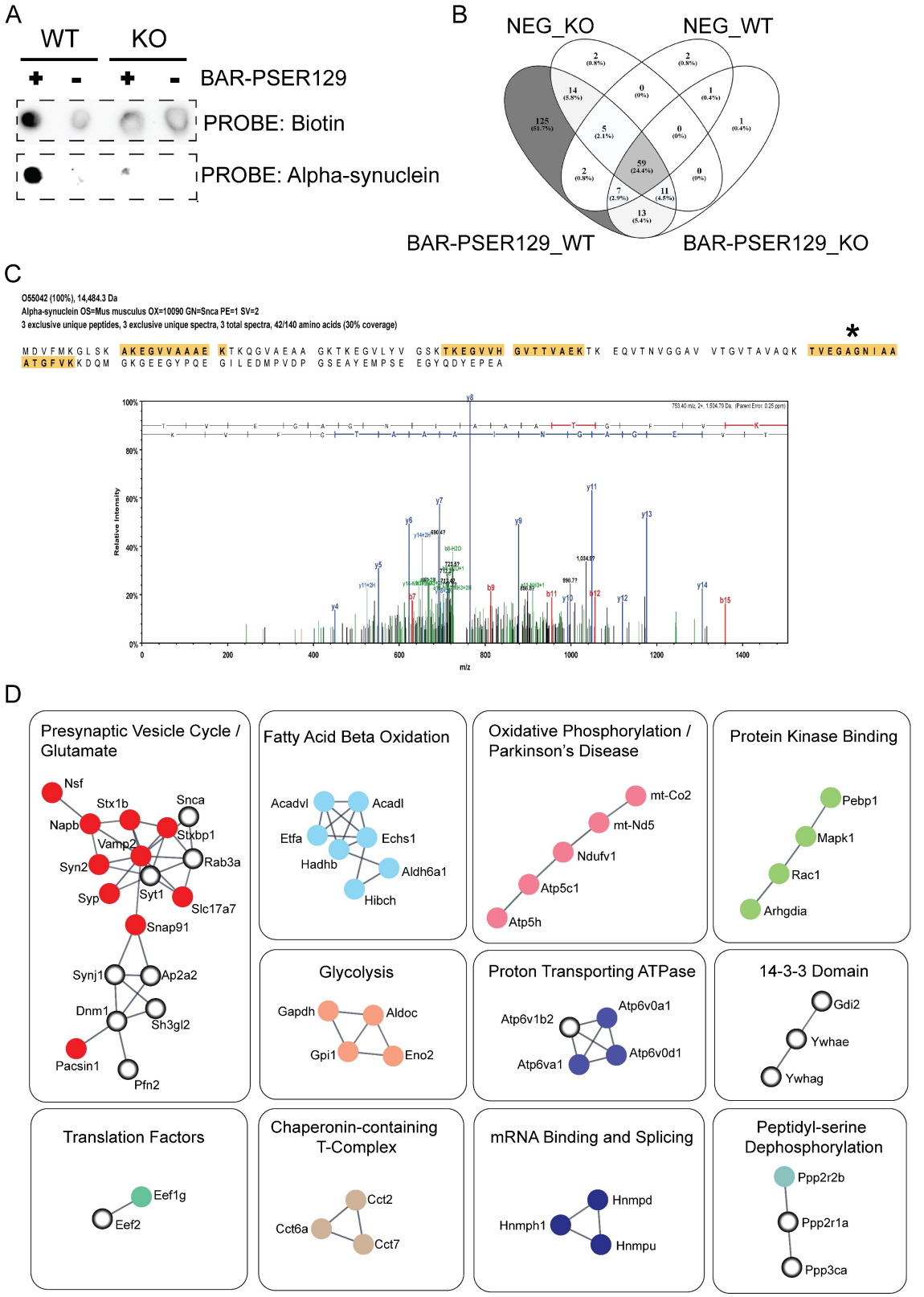
A
WT
KO
+ - + - BAR-PSER129
PROBE: Biotin
PROBE: Alpha-synuclein
B
NEG_KO
NEG_WT
BAR-PSER129_WT
BAR-PSER129_KO
125 (51.7%)
14 (5.8%)
2 (0.8%)
0 (0%)
2 (0.8%)
1 (0.4%)
5 (2.1%)
0 (0%)
1 (0.4%)
2 (0.8%)
59 (24.4%)
0 (0%)
7 (2.9%)
11 (4.5%)
13 (5.4%)
C
O55042 (100%), 14,484.3 Da
Alpha-synuclein OS=Mus musculus OX=10090 GN=Snca PE=1 SV=2
3 exclusive unique peptides, 3 exclusive unique spectra, 3 total spectra, 42/140 amino acids (30% coverage)
MDVFMKGLSK AKEGVVAAAE KTKQGVAEAA GKTKEGVLYV GSKTKEGVVH GVTTVAEKTK EQVTNVGGAV VTGVTAVAQK TVEGAGNIAA
ATGFVKKDQM GKGEEGYPQE GILEDMPVDP GSEAYEMPSE EGYQDYEPEA
*
Relative Intensity
m/z
D
Presynaptic Vesicle Cycle / Glutamate
Nsf
Stx1b
Snca
Napb
Stxbp1
Vamp2
Rab3a
Syn2
Syt1
Syp
Slc17a7
Snap91
Synj1
Ap2a2
Dnm1
Sh3gl2
Pacsin1
Pfn2
Fatty Acid Beta Oxidation
Acadvl
Acadl
Etfa
Echs1
Hadhb
Aldh6a1
Hibch
Oxidative Phosphorylation / Parkinson's Disease
mt-Co2
mt-Nd5
Ndufv1
Atp5c1
Atp5h
Protein Kinase Binding
Pebp1
Mapk1
Rac1
Arhgdia
Glycolysis
Gapdh
Aldoc
Gpi1
Eno2
Proton Transporting ATPase
Atp6v1b2
Atp6v0a1
Atp6va1
Atp6v0d1
14-3-3 Domain
Gdi2
Ywhae
Ywhag
Translation Factors
Eef1g
Eef2
Chaperonin-containing T-Complex
Cct2
Cct6a
Cct7
mRNA Binding and Splicing
Hnmpd
Hnmph1
Hnmpu
Peptidyl-serine Dephosphorylation
Ppp2r2b
Ppp2r1a
Ppp3ca

717 **Figure 6.** PSER129 interactome in mouse OB. BAR-PSER129 was conducted on brain sections
718 from WT and KO mice. A primary antibody omission control was conducted for each sample
719 ("Neg") where the sample were processed in the absence of PSER129 antibody. (A) Spot blot of
720 the captured proteins were probed for biotinylated proteins or alpha-synuclein. Resulting
721 chemiluminescent detection is shown. (B) Samples were analyzed by LC-MS/MS. Venn diagram
722 depicts overlap of identified proteins between samples. 125 proteins were identified exclusively in
723 the BAR-PSER129 WT sample. (C) Alpha-synuclein identification in the BAR-PSER129 capture
724 sample. Three high confidence peptides (highlighted yellow) were identified. Spectrum from the
725 most abundant alpha-synuclein peptide identified. (Denoted by an asterisk). (D) STRING
726 analysis and MCL clustering of the 125 proteins identified. High confidence functional interactions
727 shown (>0.7). Proteins lacking high confidence functional interactions are not shown. Enrichment
728 analysis was performed for each distinct STRING cluster and a consensus-enriched term(s) were
729 manually annotated above each cluster. Protein nodes colored for easy visualization of each
730 cluster. Open-circle nodes indicate alpha-synuclein interactors previously identified in rat primary
731 cortical neurons using *in vivo* proximity labeling methods (25).
732
733
734

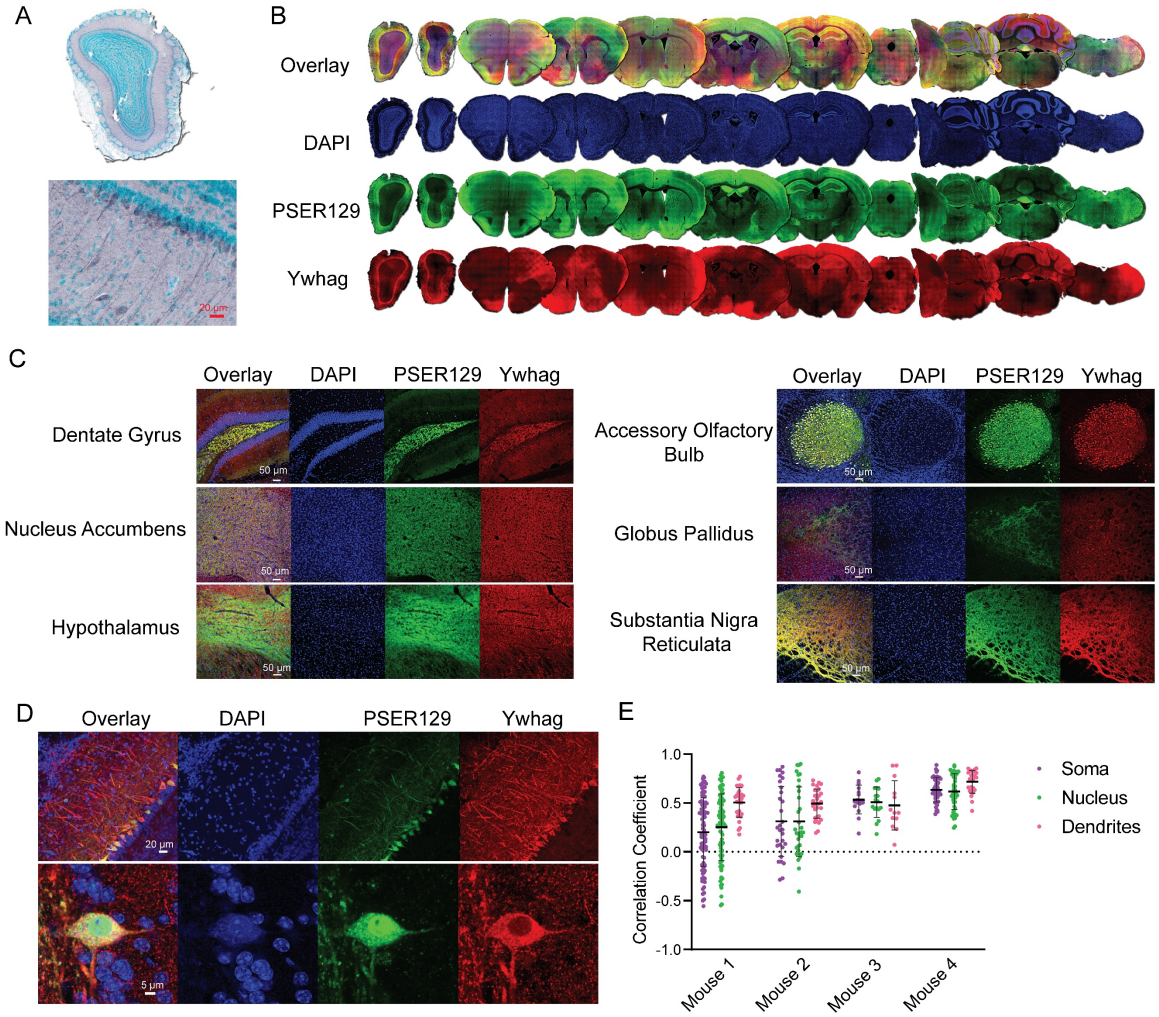

Figure 7. BAR-PSER129 identified protein Ywhag associated with PSER129 across the neuroaxis. (A) IHC detection of Ywhag in the WT mouse OB. (B) Whole section scans of dual-labeled Ywhag and PSER129 across the neuroaxis of a healthy mouse. (C) High magnification confocal images of Ywhag and PSER129 in select brain regions. (D) High magnification confocal images of Ywhag and PSER129 in the mitral cell layer. (E) Colocalization analysis of mitral cells. Pearson's correlation coefficient was calculated in the soma, nucleus, and dendrites of PSER129 positive mitral cells. (WT mice, n=4).

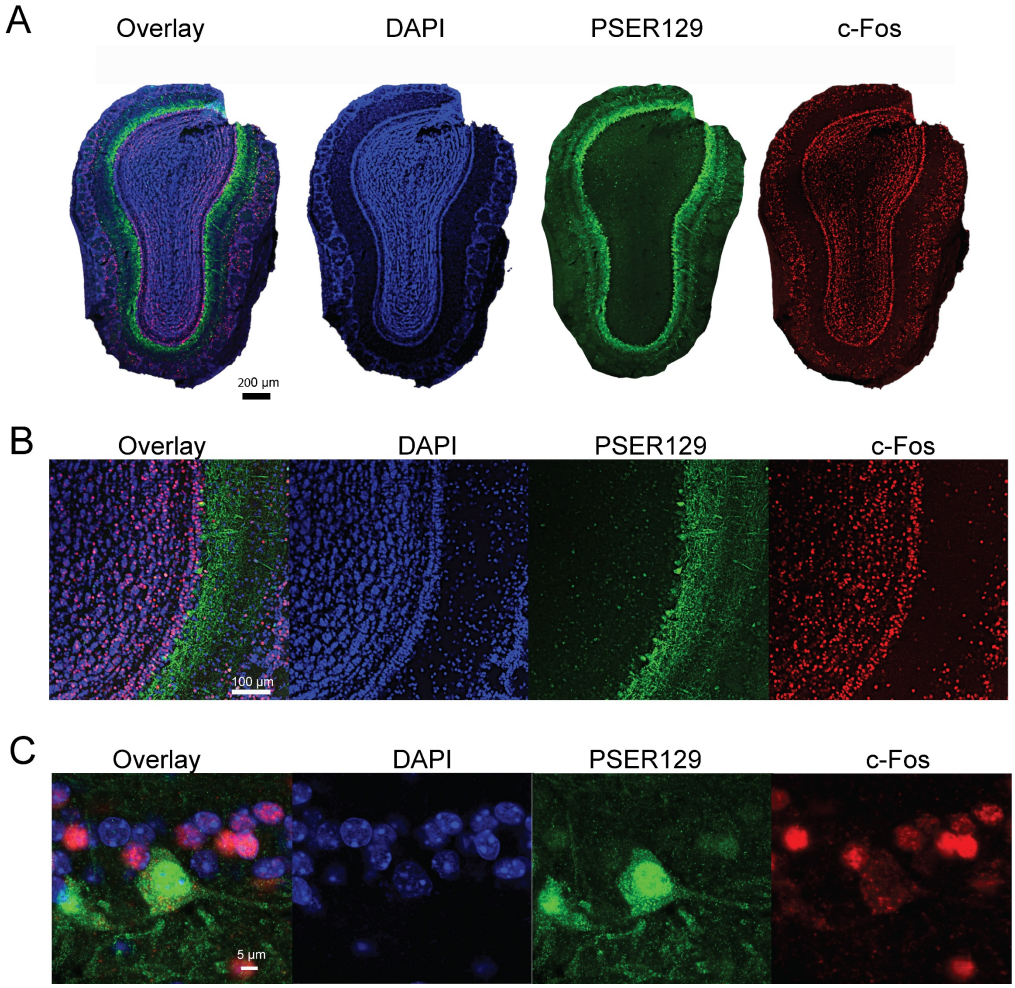

Figure 8. PSER129 positive mitral cells are c-Fos negative. The OB from WT mice were labeled for PSER129 and neuronal activity marker c-Fos. (A) Whole section confocal scans of labeled OB. (B) High magnification confocal images of mitral cell layer. (C) Expanded high magnification images of a single PSER129 positive mitral cell. (WT mice, n=4).

759 **Table 1.** List of Specimens and Summary of Results. * Antibody EP1536Y was used to detect
760 PSER129 in the OB. 0 means PSER129 positive cells were not observed in the mitral cell layer
761 and 1 denotes PSER129 positive cells were observed in the mitral cell layer. Only staining
762 conditions without proteinase K were considered. †TBX21 is a mitral cell marker. 0 means no
763 staining and 1 means staining. ‡Specimen 25 was euthanized early due to post op-right subdural
764 hematoma. §Specimen 36 had weak TBX-21 staining but was observed in the citrate retrieval
765 condition.
766

#	Species	Sex	Age at death (yrs)	Method of fixation	Strain	Genotype	EP1536Y staining*	TBX21 staining†	Disease
1	*Mus musculus*	M	0.66	PF/DF	C57BL/6J	α-syn KO	0	1	NA
2	*Mus musculus*	M	0.66	PF/DF	C57BL/6J	α-syn KO	0	1	NA
3	*Mus musculus*	M	0.66	PF/DF	C57BL/6J	α-syn KO	0	1	NA
4	*Mus musculus*	M	0.66	PF/DF	C57BL/6J	α-syn KO	0	1	NA
5	*Mus musculus*	M	0.66	PF/DF	C57BL/6J	WT	1	1	NA
6	*Mus musculus*	M	0.66	PF/DF	C57BL/6J	WT	1	1	NA
7	*Mus musculus*	M	0.66	PF/DF	C57BL/6J	WT	0	1	NA
8	*Mus musculus*	M	0.66	PF/DF	C57BL/6J	WT	1	1	NA
9	*Mus musculus*	M	0.83	PF/DF	C57BL/6J	WT	1	ND	NA
10	*Mus musculus*	M	0.83	PF/DF	C57BL/6J	WT	1	ND	NA
11	*Mus musculus*	M	0.83	PF/DF	C57BL/6J	WT	1	ND	NA
12	*Mus musculus*	F	0.66	PF/DF	C57BL/6J	α-syn KO	0	1	NA
13	*Mus musculus*	F	0.66	PF/DF	C57BL/6J	α-syn KO	0	1	NA
14	*Mus musculus*	F	0.66	PF/DF	C57BL/6J	α-syn KO	0	1	NA
15	*Mus musculus*	F	0.66	PF/DF	C57BL/6J	WT	1	1	NA
16	*Mus musculus*	F	0.66	PF/DF	C57BL/6J	WT	1	1	NA
17	*Mus musculus*	F	0.66	PF/DF	C57BL/6J	WT	1	1	NA

18	*Mus musculus*	F	0.66	PF/DF	C57BL/6J	WT	1	1	NA
19	*Mus musculus*	F	0.66	PF/DF	C57BL/6J	WT	1	1	NA
20	*Mus musculus*	F	0.83	PF/DF	C57BL/6J	WT	1	ND	NA
21	*Mus musculus*	F	0.83	PF/DF	C57BL/6J	WT	1	ND	NA
22	*Rattus norvegicus domestica*	NA	1.33	DF	SD	WT	0	1	NA
23	*Rattus norvegicus domestica*	NA	1.33	DF	SD	WT	1	1	NA
24	*Rattus norvegicus domestica*	NA	1.33	DF	SD	WT	1	1	NA
‡25	*Macaca fascicularis*	M	10.86	PF/DF	NA	WT	1	1	NA
26	*Macaca fascicularis*	F	5.59	PF/DF	NA	WT	1	1	NA
27	*Homo sapiens*	M	93.24	DF	NA	NA	0	0	NS
28	*Homo sapiens*	M	87.8	DF	NA	NA	0	ND	NS
29	*Homo sapiens*	F	74.1	DF	NA	NA	0	0	NS
30	*Homo sapiens*	F	87	DF-Paraffin	NA	NA	1	1	NS
31	*Homo sapiens*	NK	NK	DF	NA	NA	0	0	PD/DLB
32	*Homo sapiens*	NK	NK	DF	NA	NA	0	0	PD/DLB
33	*Homo sapiens*	NK	NK	DF	NA	NA	0	0	PD/DLB
34	*Homo sapiens*	NK	NK	DF	NA	NA	0	0	PD/DLB
35	*Homo sapiens*	NK	NK	DF	NA	NA	0	0	PD/DLB
§36	*Homo sapiens*	NK	NK	DF	NA	NA	1	1	PD/DLB

NA: not assessed; NK: Not Known; NS: non-synucleinopathy; ND: not determined; PF/DF: Perfusion fixation/Drop fixation.

References

1. Braak H*, et al.* (2003) Staging of brain pathology related to sporadic Parkinson's disease. *Neurobiol Aging* 24(2):197-211.
2. Beach TG*, et al.* (2009) Unified staging system for Lewy body disorders: correlation with nigrostriatal degeneration, cognitive impairment and motor dysfunction. *Acta Neuropathol* 117(6):613-634.
3. Beach TG*, et al.* (2010) Multi-organ distribution of phosphorylated alpha-synuclein histopathology in subjects with Lewy body disorders. *Acta Neuropathol* 119(6):689-702.
4. Beach TG*, et al.* (2009) Olfactory bulb alpha-synucleinopathy has high specificity and sensitivity for Lewy body disorders. *Acta Neuropathol* 117(2):169-174.
5. Sengoku R*, et al.* (2008) Incidence and extent of Lewy body-related alpha-synucleinopathy in aging human olfactory bulb. *Journal of neuropathology and experimental neurology* 67(11):1072-1083.
6. Olichney JM*, et al.* (2005) Anosmia is very common in the Lewy body variant of Alzheimer's disease. *J Neurol Neurosurg Psychiatry* 76(10):1342-1347.
7. Ross GW*, et al.* (2008) Association of olfactory dysfunction with risk for future Parkinson's disease. *Ann Neurol* 63(2):167-173.
8. Chiba Y*, et al.* (2012) Retrospective survey of prodromal symptoms in dementia with Lewy bodies: comparison with Alzheimer's disease. *Dement Geriatr Cogn Disord* 33(4):273-281.
9. Fujishiro H*, et al.* (2013) Dementia with Lewy bodies: early diagnostic challenges. *Psychogeriatrics* 13(2):128-138.
10. Braak H*, et al.* (2006) Stanley Fahn Lecture 2005: The staging procedure for the inclusion body pathology associated with sporadic Parkinson's disease reconsidered. *Movement Disorders* 21(12):2042-2051.
11. Rey NL, Wesson DW, & Brundin P (2018) The olfactory bulb as the entry site for prion-like propagation in neurodegenerative diseases. *Neurobiol Dis* 109(Pt B):226-248.
12. Shahmoradian SH*, et al.* (2019) Lewy pathology in Parkinson's disease consists of crowded organelles and lipid membranes. *Nat Neurosci* 22(7):1099-1109.
13. den Jager WA (1969) Sphingomyelin in Lewy inclusion bodies in Parkinson's disease. *Arch Neurol* 21(6):615-619.
14. Lashuel HA*, et al.* (2022) Revisiting the specificity and ability of phospho-S129 antibodies to capture alpha-synuclein biochemical and pathological diversity. *NPJ Parkinsons Dis* 8(1):136.
15. Fujiwara H*, et al.* (2002) alpha-Synuclein is phosphorylated in synucleinopathy lesions. *Nat Cell Biol* 4(2):160-164.
16. Delic V*, et al.* (2018) Sensitivity and specificity of phospho-Ser129 alpha-synuclein monoclonal antibodies. *J Comp Neurol* 526(12):1978-1990.
17. Ivell R, Teerds K, & Hoffman GE (2014) Proper application of antibodies for immunohistochemical detection: antibody crimes and how to prevent them. *Endocrinology* 155(3):676-687.
18. Cave JW, Fujiwara N, Weibman AR, & Baker H (2016) Cytoarchitectural changes in the olfactory bulb of Parkinson's disease patients. *NPJ Parkinsons Dis* 2:16011.

814 19. Mahul-Mellier AL*, et al.* (2020) The process of Lewy body formation, rather than simply
815 alpha-synuclein fibrillization, is one of the major drivers of neurodegeneration. *Proc Natl*
816 *Acad Sci U S A* 117(9):4971-4982.
817 20. Lashuel HA*, et al.* (2022) Revisiting the specificity and ability of phospho-S129 antibodies
818 to capture alpha-synuclein biochemical and pathological diversity. *npj Parkinson's*
819 *Disease* 8(1):136.
820 21. Moors TE*, et al.* (2021) The subcellular arrangement of alpha-synuclein proteoforms in
821 the Parkinson's disease brain as revealed by multicolor STED microscopy. *Acta*
822 *Neuropathol* 142(3):423-448.
823 22. Schmidt MF, Gan ZY, Komander D, & Dewson G (2021) Ubiquitin signalling in
824 neurodegeneration: mechanisms and therapeutic opportunities. *Cell Death &*
825 *Differentiation* 28(2):570-590.
826 23. Kuzuhara S, Mori H, Izumiyama N, Yoshimura M, & Ihara Y (1988) Lewy bodies are
827 ubiquitinated. A light and electron microscopic immunocytochemical study. *Acta*
828 *Neuropathol* 75(4):345-353.
829 24. Killinger BA*, et al.* (2022) In situ proximity labeling identifies Lewy pathology molecular
830 interactions in the human brain. *Proceedings of the National Academy of Sciences*
831 119(5):e2114405119.
832 25. Chung CY*, et al.* (2017) In Situ Peroxidase Labeling and Mass-Spectrometry Connects
833 Alpha-Synuclein Directly to Endocytic Trafficking and mRNA Metabolism in Neurons. *Cell*
834 *Syst* 4(2):242-250 e244.
835 26. Kawamoto Y*, et al.* (2002) 14-3-3 Proteins in Lewy Bodies in Parkinson Disease and
836 Diffuse Lewy Body Disease Brains. *Journal of Neuropathology & Experimental Neurology*
837 61(3):245-253.
838 27. McFarland MA, Ellis CE, Markey SP, & Nussbaum RL (2008) Proteomics analysis identifies
839 phosphorylation-dependent alpha-synuclein protein interactions. *Mol Cell Proteomics*
840 7(11):2123-2137.
841 28. Killinger BA, Melki R, Brundin P, & Kordower JH (2019) Endogenous alpha-synuclein
842 monomers, oligomers and resulting pathology: let's talk about the lipids in the room.
843 *NPJ Parkinsons Dis* 5:23.
844 29. Wu Q*, et al.* (2020) Neuronal activity modulates alpha-synuclein aggregation and
845 spreading in organotypic brain slice cultures and in vivo. *Acta Neuropathol* 140(6):831-
846 849.
847 30. Fortin DL*, et al.* (2005) Neural activity controls the synaptic accumulation of alpha-
848 synuclein. *J Neurosci* 25(47):10913-10921.
849 31. Daniel SE & Hawkes CH (1992) Preliminary diagnosis of Parkinson's disease by olfactory
850 bulb pathology. *Lancet* 340(8812):186.
851 32. Ubeda-Banon I*, et al.* (2010) alpha-Synucleinopathy in the human olfactory system in
852 Parkinson's disease: involvement of calcium-binding protein- and substance P-positive
853 cells. *Acta Neuropathol* 119(6):723-735.
854 33. Kovacs T, Papp MI, Cairns NJ, Khan MN, & Lantos PL (2003) Olfactory bulb in multiple
855 system atrophy. *Mov Disord* 18(8):938-942.
856 34. Hubbard PS, Esiri MM, Reading M, McShane R, & Nagy Z (2007) Alpha-synuclein
857 pathology in the olfactory pathways of dementia patients. *J Anat* 211(1):117-124.
858 35. Hallacli E*, et al.* (2022) The Parkinson's disease protein alpha-synuclein is a modulator of
859 processing bodies and mRNA stability. *Cell* 185(12):2035-2056 e2033.

860 36. Sawamura M*, et al.* (2022) α-synuclein propagation via olfactory pathway induces
861 olfactory bulb atrophy and widespread glucose hypometabolism in a non-human
862 primate model. (P1-1.Virtual). *Neurology* 98(18 Supplement):2422.
863 37. Tremblay C*, et al.* (2022) Effect of olfactory bulb pathology on olfactory function in
864 normal aging. *Brain Pathol*:e13075.
865 38. Abd-Elhadi S*, et al.* (2015) Total and Proteinase K-Resistant alpha-Synuclein Levels in
866 Erythrocytes, Determined by their Ability to Bind Phospholipids, Associate with
867 Parkinson's Disease. *Sci Rep* 5:11120.
868 39. Bell R & Vendruscolo M (2021) Modulation of the Interactions Between alpha-Synuclein
869 and Lipid Membranes by Post-translational Modifications. *Front Neurol* 12:661117.
870 40. Scott JW, McBride RL, & Schneider SP (1980) The organization of projections from the
871 olfactory bulb to the piriform cortex and olfactory tubercle in the rat. *J Comp Neurol*
872 194(3):519-534.
873 41. Taguchi K, Watanabe Y, Tsujimura A, & Tanaka M (2019) Expression of alpha-synuclein is
874 regulated in a neuronal cell type-dependent manner. *Anat Sci Int* 94(1):11-22.
875 42. Taguchi K, Watanabe Y, Tsujimura A, & Tanaka M (2016) Brain region-dependent
876 differential expression of alpha-synuclein. *J Comp Neurol* 524(6):1236-1258.
877 43. Zhou J*, et al.* (2011) Changes in the solubility and phosphorylation of alpha-synuclein
878 over the course of Parkinson's disease. *Acta Neuropathol* 121(6):695-704.
879 44. Del Tredici K, Rub U, De Vos RA, Bohl JR, & Braak H (2002) Where does parkinson
880 disease pathology begin in the brain? *Journal of neuropathology and experimental*
881 *neurology* 61(5):413-426.
882 45. Hoogland PV, van den Berg R, & Huisman E (2003) Misrouted olfactory fibres and
883 ectopic olfactory glomeruli in normal humans and in Parkinson and Alzheimer patients.
884 *Neuropathol Appl Neurobiol* 29(3):303-311.
885 46. Ubeda-Banon I, Flores-Cuadrado A, Saiz-Sanchez D, & Martinez-Marcos A (2017)
886 Differential Effects of Parkinson's Disease on Interneuron Subtypes within the Human
887 Anterior Olfactory Nucleus. *Front Neuroanat* 11:113.
888 47. Marin C*, et al.* (2022) Olfactory Bulb Excitotoxicity as a Gap-Filling Mechanism
889 Underlying the Link Between Traumatic Brain Injury-Induced Secondary Neuronal
890 Degeneration and Parkinson's Disease-Like Pathology. *Neurochem Res* 47(4):1025-1036.
891 48. Chen F*, et al.* (2021) alpha-Synuclein aggregation in the olfactory bulb induces olfactory
892 deficits by perturbing granule cells and granular-mitral synaptic transmission. *NPJ*
893 *Parkinsons Dis* 7(1):114.
894 49. Courte J*, et al.* (2020) The expression level of alpha-synuclein in different neuronal
895 populations is the primary determinant of its prion-like seeding. *Sci Rep* 10(1):4895.
896 50. Alam MM*, et al.* (2022) Alpha synuclein, the culprit in Parkinson disease, is required for
897 normal immune function. *Cell Rep* 38(2):110090.
898 51. Kok EH*, et al.* (2021) Alpha-synuclein pathology of olfactory bulbs/peduncles in the
899 Vantaa85+ cohort exhibit two divergent patterns: a population-based study. *Acta*
900 *Neuropathol* 142(4):777-780.
901 52. Horsager J*, et al.* (2020) Brain-first versus body-first Parkinson's disease: a multimodal
902 imaging case-control study. *Brain* 143(10):3077-3088.
903 53. Borghammer P*, et al.* (2022) A postmortem study suggests a revision of the dual-hit
904 hypothesis of Parkinson's disease. *NPJ Parkinsons Dis* 8(1):166.

905 54. Sengoku R*, et al.* (2008) Incidence and Extent of Lewy Body-Related α-Synucleinopathy
906 in Aging Human Olfactory Bulb. *Journal of Neuropathology & Experimental Neurology*
907 67(11):1072-1083.
908 55. Niu H*, et al.* (2020) IL-1beta/IL-1R1 signaling induced by intranasal lipopolysaccharide
909 infusion regulates alpha-Synuclein pathology in the olfactory bulb, substantia nigra and
910 striatum. *Brain Pathol* 30(6):1102-1118.
911 56. Arawaka S, Sato H, Sasaki A, Koyama S, & Kato T (2017) Mechanisms underlying
912 extensive Ser129-phosphorylation in α-synuclein aggregates. *Acta Neuropathologica*
913 *Communications* 5(1):48.
914 57. Arnsten AFT*, et al.* (2019) Alzheimer's-like pathology in aging rhesus macaques: Unique
915 opportunity to study the etiology and treatment of Alzheimer's disease. *Proc Natl Acad*
916 *Sci U S A*.
917 58. Arawaka S, Sato H, Sasaki A, Koyama S, & Kato T (2017) Mechanisms underlying
918 extensive Ser129-phosphorylation in alpha-synuclein aggregates. *Acta Neuropathol*
919 *Commun* 5(1):48.
920 59. Zhang W*, et al.* (2017) Fully automated 5-plex fluorescent immunohistochemistry with
921 tyramide signal amplification and same species antibodies. *Lab Invest* 97(7):873-885.
922 60. Lyu Q, Zheng HS, Laprocina K, & Huang CC (2020) Microwaving and Fluorophore-
923 Tyramide for Multiplex Immunostaining on Mouse Adrenals - Using Unconjugated
924 Primary Antibodies from the Same Host Species. *J Vis Exp* (156).
925 61. Wessel D & Flugge UI (1984) A method for the quantitative recovery of protein in dilute
926 solution in the presence of detergents and lipids. *Anal Biochem* 138(1):141-143.

927

Supplementary Information for

Distribution of phosphorylated alpha-synuclein in non-diseased brain implicates olfactory bulb mitral cells in synucleinopathy pathogenesis

Bryan A. Killinger[a], Gabriela Mercado[b], Solji Choi[a], Yaping Chu[C], Tyler Tittle[C], Patrik Brundin[b,d], and Jeffrey H. Kordower[C]

[a]Graduate College, Rush University Medical Center, Chicago Illinois 60612

[b] Parkinson's disease Center, Department of Neurodegenerative Science, Van Andel Institute, Grand Rapids MI 49503

[c] ASU-Banner Neurodegenerative Disease Research Center (NDRC), Arizona State University, Tempe Arizona 85287

[d]Pharma Research and Early Development (pRED), F Hoffman-La Roche, New York, USA

*Bryan A. Killinger

Email: bryan_killinger@rush.edu

This PDF file includes:

Supplementary text
Figures S1 to S9
Legends for Datasets S1 to S5
SI References

Other supplementary materials for this manuscript include the following:

Datasets S1 to S5

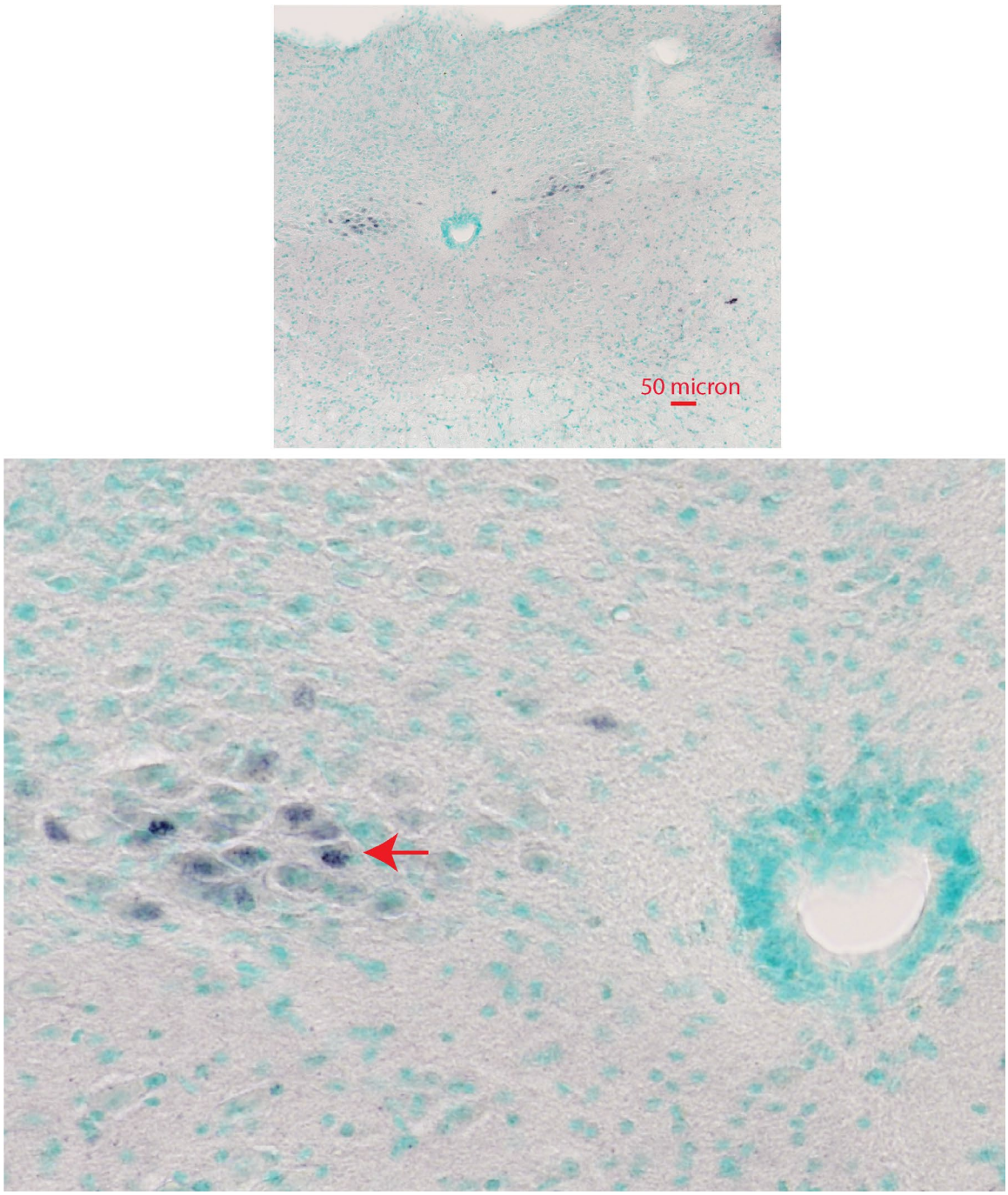

Figure S1. PSER129 immunoreactivity in the dorsal motor nucleus of the vagus (DMNV). PSER129 staining was absent from the brainstem and cerebellum of wildtype mice except for immunoreactivity of a small group of cells in the DMNV shown here. Red arrow highlights the reactive cells.

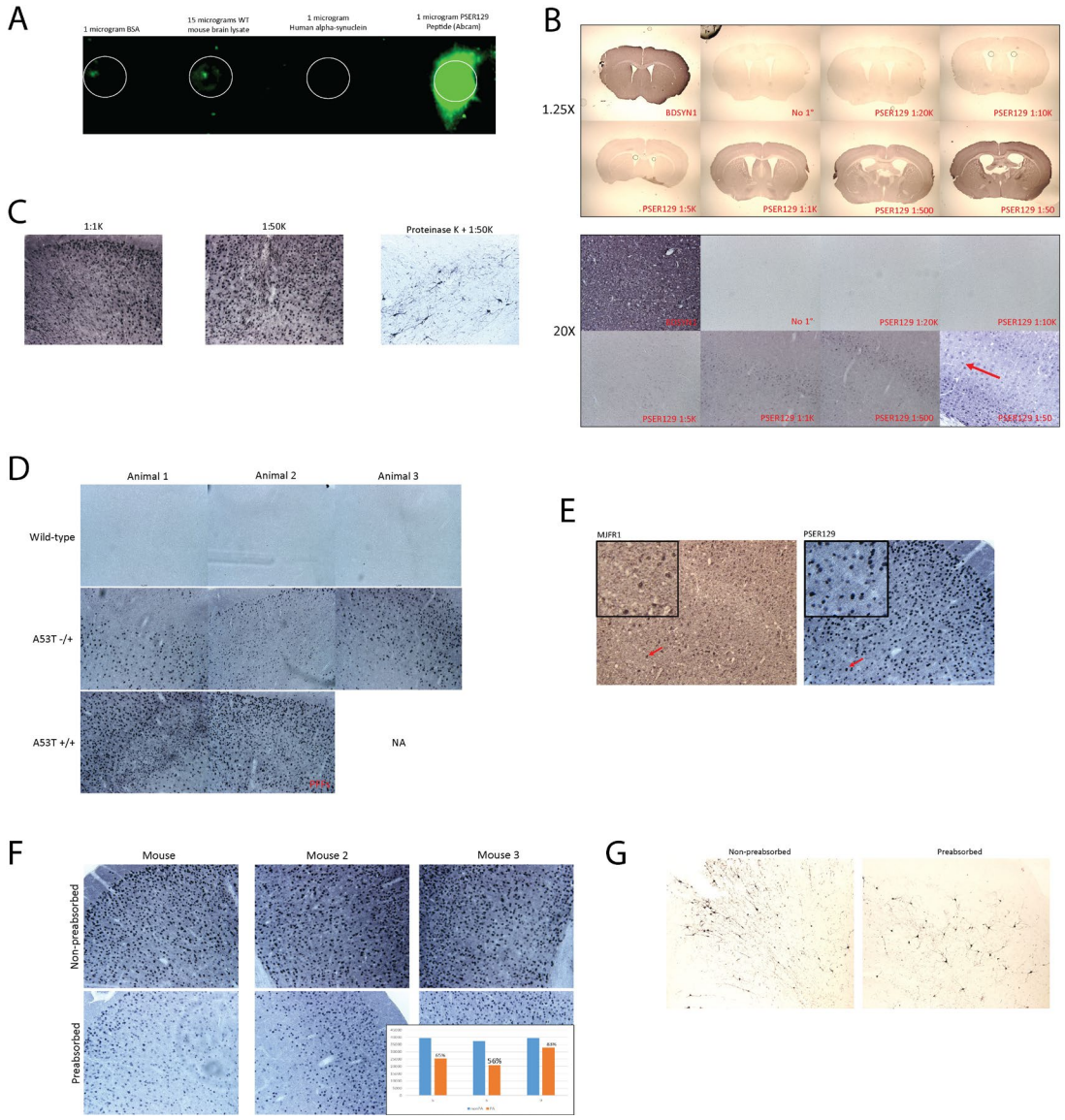

Figure S2. Validation Experiments in M83 mice and WT mice. (A) Dot-blot demonstrates EP1536Y reactivity against several samples of interest. (B) EP1536Y dilution experiments. Brain sections from wild-type mice were probed with the antibody BDSYN1 (total synuclein) or several dilutions of EP1536Y and developed with DAB or nickel enhanced DAB. Low and high magnification images of the resulting reactivity. Higher dilutions were required to avoid perfuse reactivity in the brain. (D) PSER129 reactivity in WT and A53T alpha-synuclein overexpressing mice (M83). At high dilutions, PSER129 reactivity was seen throughout the M83 brain. (E) Antibody MJFR1 only reacts to human alpha-synuclein. M83 mice show similar tissue distribution of human alpha-synuclein as PSER129 tissues distribution. This suggests that expressed human alpha-synuclein is phosphorylated. (F) Preabsorption of EP1536Y antibody. The antibody was preaborbed against excesses alpha-synuclein phosphopeptide (abcam). The preabsorbed antibody was then used to stain brain sections from M83 mice not bearing alpha-synuclein pathology. Results show a reduction in signal following preabsorbtion, but not a loss of staining, typical of monoclonal antibody reactivity. (G) Preabsorbed antibody was used to stain proteinase K treated M83 mouse brains baring alpha-synuclein pathology. Similarly, pathology detection was inhibited with preabsorbtion, but not eliminated.

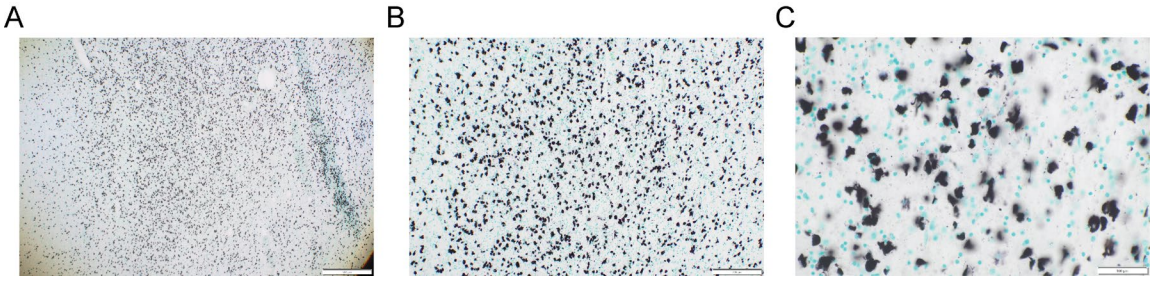

Figure S3. PSER129 content in multiple systems atrophy(MSA) tissue section used for positive control in Fig. 1. Free-floating striatal section from MSA brain stained for PSER129 using antibody EP1536Y. Sections were counterstained with methyl green. Images acquired with a (A) 4X (B) 10X and (C) 20X objective. Dense glial cytoplasmic inclusions were observed predominantly in white matter of the tissue section.

Non-human Primate

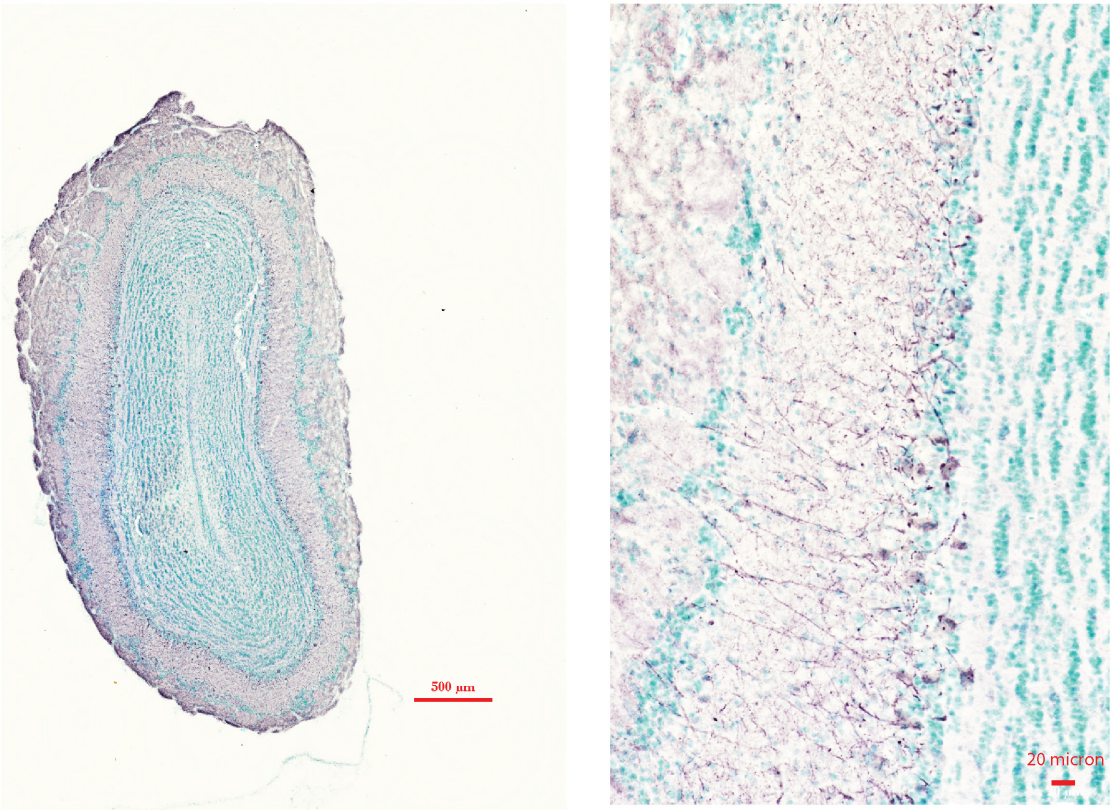

Figure S4 Antibody pSyn#64 reactivity in OB of a healthy non-human primate. Formalin fixed floating coronal sections from a cynomolgus monkey were incubated with mouse monoclonal antibody pSyn#64 (FuJIFILM Wako Pure Chemical Corporation) diluted 1:10K and detected using tyramine signal amplification. Sections were counterstained with methyl green. The left image depicts a whole section scan, and the left image depicts an image taken with a 20X objective. Scale bars are depicted on each image.

<

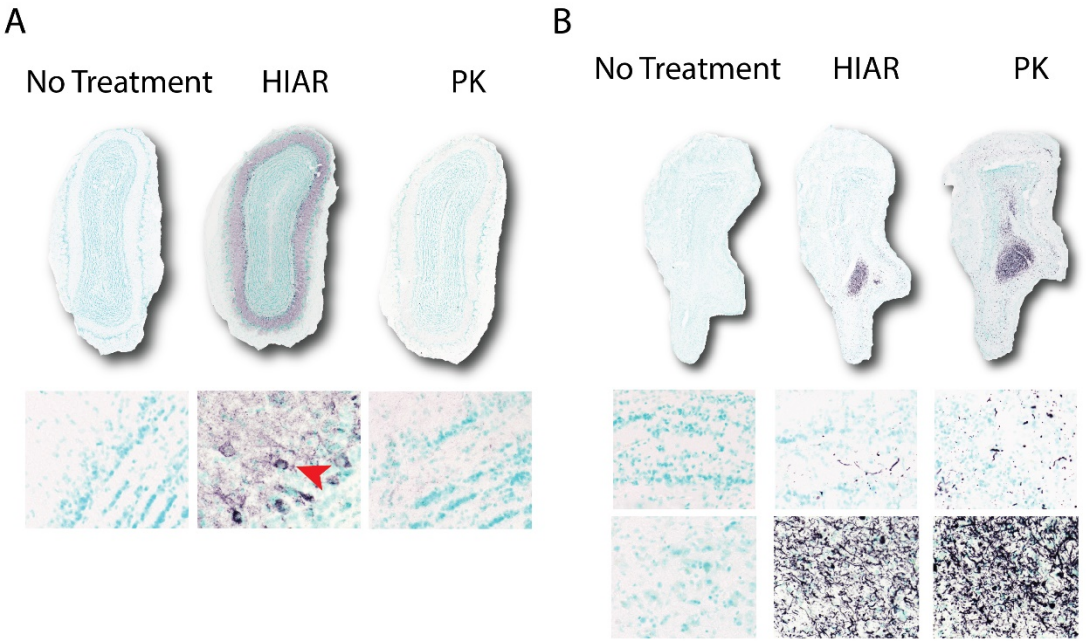

Figure S5. Detection of PSER129 is dependent on antigen retrieval techniques. OB sections from a non-human primate (A) and individual with Parkinson's disease (B) were immunostained using the EP1536Y antibody under different tissue processing conditions. For the "no treatment" condition tissues were stained as floating sections without antigen retrieval. For "HIAR" tissues were mounted onto slides and heated to ~95°C in citrate buffer for 30 min. For "PK" samples were mounted onto slides and treated with 20 µg/mL proteinase K for 10 min at 37°C. Resulting EP1536Y immunoreactivity for each condition is depicted. Red arrow highlights PSER129 reactivity in mitral cells.

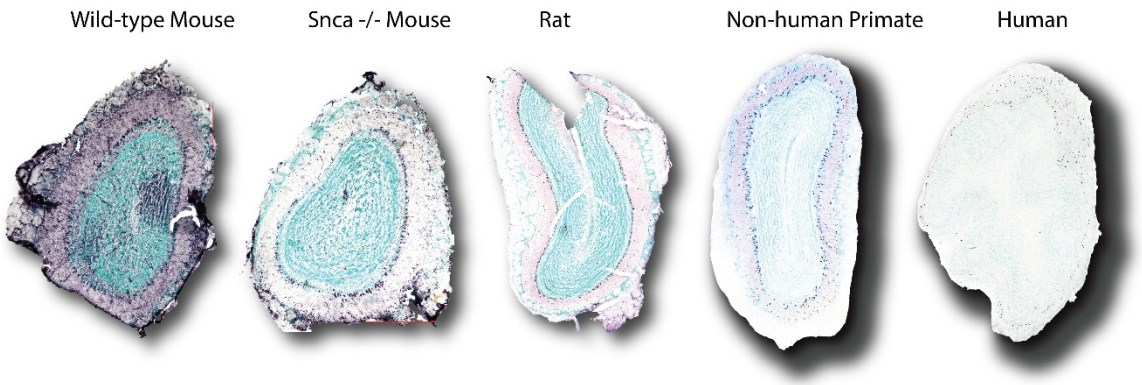

Figure S6. TBX21 reactivity in the OB. Immunoreactivity of mitral cell marker TBX21 in OB specimens from each species assessed in this study. TBX21 reactivity was observed in the mitral cell layer across species. High background was observed in the mouse specimens because the anti-TBX21 antibody was of mouse origin.

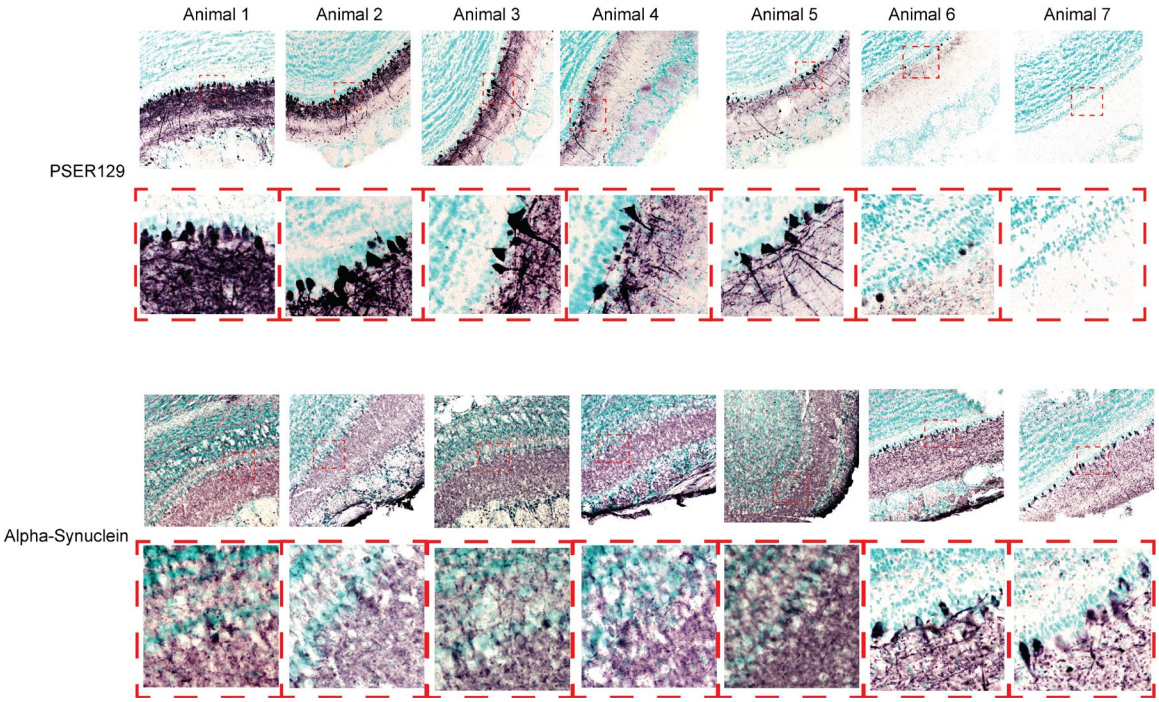

Figure S7. PSER129 and Alpha-synuclein in OB mitral cell layer of WT mice. PSER129 and alpha-synuclein were stained in WT mice OB's using antibodies EP1536Y (Abcam) and SYN1 (BDbiosciences), respectively. Nickle-DAB was used as a chromogen and sections were counterstained with methyl green. Images were acquired using a 20X objective. Enlarged images of mitral cell layer are depicted in bottom panels and position of enlarged image denoted by a red dotted box. N=7 WT mice.

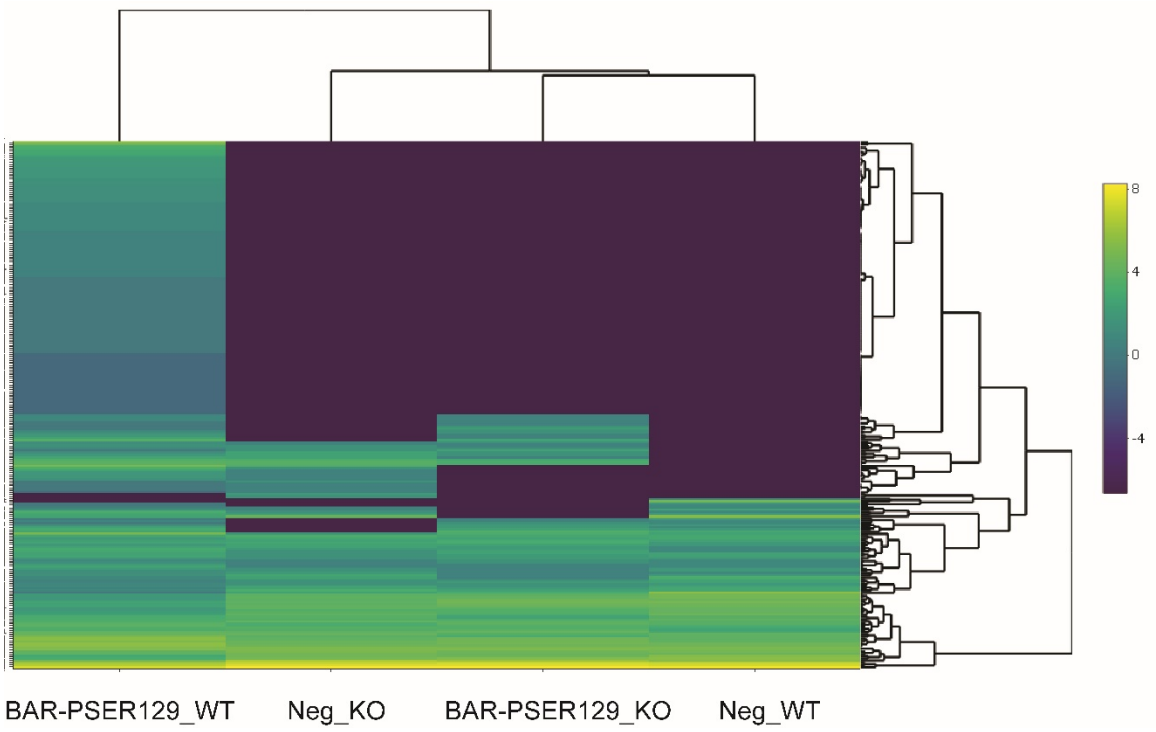

Figure S8. Heatmap of proteins identified in each BAR sample. BAR was conducted on tissue sections from non-diseased wildtype (WT) and alpha-synuclein knockout (KO) mice. BAR was conducted with anti-PSER129 (BAR-PSER129) and without primary antibody (Neg). Log2 values of relative protein abundance.

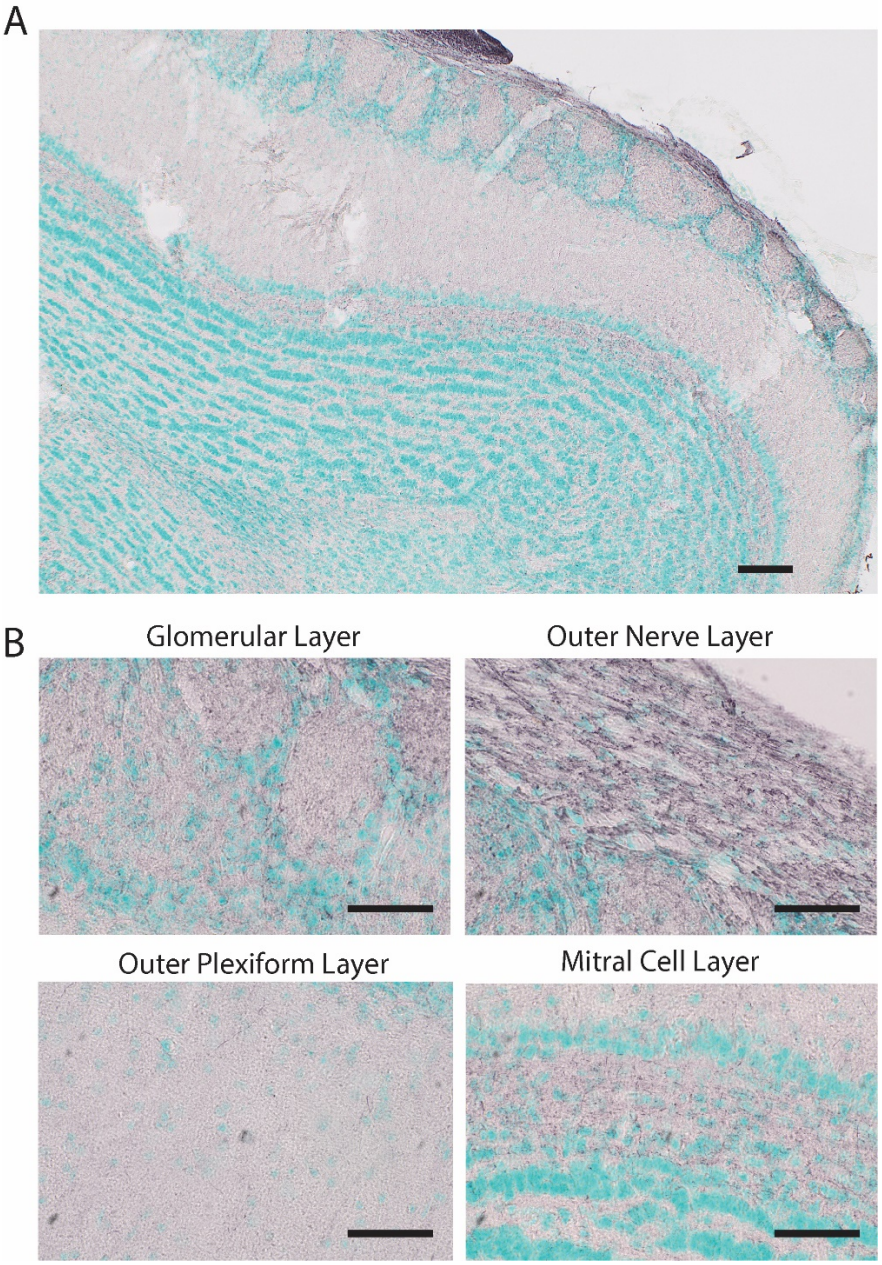

Fig S9. Phospho-Tau immunoreactivity in the mouse olfactory bulb. 40-micron floating olfactory bulb sections were incubated with anti-phospho-tau antibody EPR2731 (Abcam) diluted 1:10K and detected using ABC with Nickle-DAB Chromogen. Sections counterstained with methylgreen. (A) Representative image taken using a 4X objective. (B) Representative images taken using a 10X objective. Depicted are the glomerular layer, outer nerve layer, outer plexiform layer, and the mitral cell layer. Prominent staining observed in the inner plexiform layer, outer nerve layer, and the glomerular layer. For (A) scale bar = 200 microns. For (B) scale bars = 100 microns.

Legends for supplemental datasets

Dataset S1 (separate file). Scaffold protein report for BAR experiments. Protein level data exported from Scaffold. Sample key; 19 = BAR-PSER129-WT, 15 = Neg-WT ,12 = BAR-PSER129-KO , 18 = Neg-KO.

Dataset S2 (separate file). Peptide report for BAR experiments. Peptide level data exported from Scaffold. Sample key; 19 = BAR-PSER129-WT, 15 = Neg-WT ,12 = BAR-PSER129-KO , 18 = Neg-KO.

Dataset S3 (separate file). Proteins detected exclusively in BAR-PSER129-WT. 125 proteins detected only in the BAR-PSER129-WT sample. Accession Number, gene name, and relative abundance provided for each protein.

Dataset S4 (separate file). Enrichment results from STRING. The 125 proteins were input into STRING, and 783 significantly enriched pathways were determined.

Dataset S5 (separate file). Enrichment results from gprofiler. The 125 proteins were ranked by relative abundance and then enrichment determined by gprofiler. 436 significantly enriched pathways were determined.

Table S1 (separate file). Human OB specimens were provided by three brain banks. Banner Sun Health, Rush Alzheimer's Disease Center, and Rush Movement Disorders Brain Bank. Detailed clinical and post-mortem information is included in this excel sheet.

Table S2 (separate file). A list of antibodies used here and properties of each antibody.